January 2022

Design Of Novel High-Performance Materials For Sliding Applications

Caleb Michael Matzke

DESIGN OF NOVEL HIGH-PERFORMANCE MATERIALS FOR SLIDING APPLICATIONS

by

Caleb Michael Matzke
Bachelor of Science, University of North Dakota, 2020
Master of Science, University of North Dakota, 2022

A Thesis

Submitted to the Graduate Faculty

of the

University of North Dakota

in partial fulfillment of the requirements

for the degree of

Master of Science in Mechanical Engineering

Grand Forks, North Dakota

August
2022

Name: Caleb Matzke

Degree: Master of Science

This thesis, submitted in partial fulfillment of the requirements for the Degree of Master of Science in Mechanical Engineering from the University of North Dakota, has been read by the Faculty Advisory Committee under whom the work has been done and is hereby approved.

DocuSigned by:
Surojit Gupta

Surojit Gupta

DocuSigned by:
Yun Ji

Yun Ji

DocuSigned by:
Stephen P Berkebile

Stephen P Berkebile

This thesis is being submitted by the appointed advisory committee as having met all of the requirements of the School of Graduate Studies at the University of North Dakota and is hereby approved.

DocuSigned by:
Chris Nelson

Chris Nelson
Dean of the School of Graduate Studies

07/27/2022
Date

PERMISSION

Title Design of novel high-performance materials for sliding applications

Department Mechanical Engineering

Degree Master of Science

In presenting this thesis in partial fulfillment of the requirements for a graduate degree from the University of North Dakota, I agree that the library of this University shall make it freely available for inspection. I further agree that permission for extensive copying for scholarly purposes may be granted by the professor who supervised my thesis work or, in his absence, by the Chairperson of the department or the dean of the School of Graduate Studies. It is understood that any copying or publication or other use of this thesis or part thereof for financial gain shall not be allowed without my written permission. It is also understood that due recognition shall be given to me and to the University of North Dakota in any scholarly use which may be made of any material in my thesis.

Caleb Matzke
June 29, 2022

ACKNOWLEDGMENTS

I would like to acknowledge the U.S. Army CRADA with the University of North Dakota and NASA EPSCoR's support for these studies. I would also like to acknowledge my Advisor, Dr. Surojit Gupta, and the members of the University of North Dakota's Materials Testing Laboratory.

ABSTRACT

Break down of a material due to mechanical usage, otherwise known as wear, is a common issue that affects almost every industry as well as many commonly used goods. Components, such as bearings, can have major damage over time, especially if they are not protected by a lubricant. This thesis investigates the friction and wear behavior of high-performance materials lubricated by fuel-based lubricants. This work is divided into two parts; The first focuses on polymer matrix composites, and the second focuses on advanced ceramics. Polymers are of interest due to the ease of production and the polymer of choice for this study was polyether ether ketone (PEEK) due to its high strength and stability at high temperatures relative to other polymers. MAX and MAB phase powders were used as additives in PEEK matrix composites. The addition of the phases improved the wear performance of PEEK-based composites during dry sliding. Ethanol lubricated composites showed lower wear than dry sliding. Advanced ceramics like SiC and Si_3N_4 are widely applicable and play a major role in water-based lubricated systems. SiC and Si_3N_4 showed lower wear rate during ethanol and DI water lubrication due to formation of stable tribofilms which resisted the formation of third bodies.

TABLE OF CONTENTS

LIST OF FIGURES ix
LIST OF TABLES x
1 CHAPTER 1 - Introduction 1
1.1 References 3
2 CHAPTER 2 -Tribological behavior of PEEK composites in ethanol and fuel-based lubricants 4
2.1 Introduction 4
2.2 Experimental Design 5
2.2.1 Sample Fabrication 5
2.2.2 Microstructure, EDS, Wear Scar Analysis 6
2.2.3 Tribological Studies 6
2.3 Results and Discussion 8
2.3.1 Microstructure 8
2.3.2 Friction 9
2.3.3 Wear Rate 14
2.3.4 Wear Scars Analysis 15
2.4 Conclusions 21
2.5 References 22
3 CHAPTER 3 - Evaluation of tribological behavior of SiC and Si_3N_4 under different tribological conditions 23
3.1 Introduction 23
3.2 Experimental Design 24
3.2.1 Fabrication 24
3.2.2 Tribology 24
3.2.3 Microstructure, EDS, and Wear track analysis 25
3.3 Results and Discussion 25
3.3.1 Microstructure and Tribological Behavior 25
3.3.2 Wear Surface Analysis and Potential Mechanisms 29

3.3.2.1 Tribology during Dry Sliding 29
3.3.2.2 Tribology during DI water and Ethanol Lubrication 32
3.4 Conclusions 37
3.5 References 38

LIST OF FIGURES

Figure 2.1 Schematics of fluid delivery system for tribology study by using a syringe pump 7
Figure 2.2 Microstructure 8
Figure 2.3 Coefficient of friction of Dry sliding 9
Figure 2.4 Coefficient of friction of Ethanol Lubrication and 5 N load. 10
Figure 2.5 Coefficient of friction of Ethanol Lubrication and 10 N load. 11
Figure 2.6 Coefficient of friction of Ethanol Lubrication and 20 N load. 12
Figure 2.7 Coefficient of friction of dodecane Lubrication and 20 N load. 13
Figure 2.8 Coefficient of friction of F-24 fuel Lubrication and 20 N load 14
Figure 2.9 Calculated wear rate due to load and lubrication method 15
Figure 2.10 EDS of Dry sliding at 20 N load 16
Figure 2.11 EDS of Ethanol Lubricated at 20 N 18
Figure 2.12 EDS of dodecane Lubricated at 20 N load 19
Figure 2.13 EDS of F-24 Lubricated at 20 N load 20
Figure 3.1 Microstructure 26
Figure 3.2 Plot of friction coefficient versus distance, total wear, and friction coefficient of SiC versus alumina tribocouples under different conditions 27
Figure 3.3 Plot of friction coefficient versus distance of different types of Si_3N_4 28
Figure 3.4 Plot of wear rate and friction coefficient of different Si3N4 compositions 29
Figure 3.5 EDS under dry sliding. 31
Figure 3.6 EDS under DI water lubrication. 34
Figure 3.7 EDS under Ethanol lubrication. 36
Figure 3.8 Schematics of tribological process 37

LIST OF TABLES

Table 2.1 EDS results of PEEK and PEEK-composites due to dry sliding 17
Table 2.2 EDS Results of PEEK and PEEK-composites due to Ethanol Lubrication 19
Table 2.3 EDS Results of PEEK and PEEK-composites due to dodecane Lubrication 20
Table 2.4 EDS Results of PEEK and PEEK-composites due to F-24 Fuel Lubrication 21
Table 3.1 EDS Results of Ceramics due to dry sliding 32
Table 3.2 EDS Results of Ceramics due to DI water lubrication 35
Table 3.3 EDS Results of Ceramics due to Ethanol lubrication 37

CHAPTER 1 - Introduction

This thesis consists of three chapters. Chapter 1 which introduces the flow of the thesis and background information relevant to the proceeding chapters. Chapter 2 is focused on polymer reinforced composites designed for sliding applications. Polymers are of interest due to the ease of producing components from them. The polymer of choice for this study will be polyether ether ketone (PEEK) due to its high strength and stability at high temperatures relative to other polymers. Chapter 3 is focused on novel SiC and Si_3N_4 ceramics and their application in sliding contacts.

Progressive break down of a material due to mechanical usage, otherwise known as wear, is an all-too-common issue that affects almost every industry as well as many commonly used goods in everyday life. Engine components in automobiles like the cylinders, pistons, and crankshaft can have major damage occur over time, especially if they are not protected by a lubricant. The commonly accepted forms of wear of broken down into four groups; adhesive wear, abrasive wear, wear caused by surface fatigue, and wear due to tribochemical reactions. Damage can be caused by one of these mechanisms or in any combination.

Wear commonly undergoes three periods during sliding. These periods are referred to as run-in, steady- state, and catastrophic. Run-in is the period that builds up to steady state conditions and is important in many systems as this is when the contacting surfaces can conform

to one another. Next is the steady-state period. This is when friction is stable and accompanied by low wear rates. Finally, is the catastrophic period. This is when large wear rates are prevalent and severe damage to the substrates surface occurs. Friction values and wear rates determined during steady-state conditions are the primary indicators in characterizing long-term properties of a system. Identifying the point at which surface damage occurs is one of the most challenging aspects of analyzing failure of components [1].

Mitigating failure of components is commonly done by using lubrication to reduce the severity of both normal and shear stresses in solid surface contact [2]. Fluid lubrication is one of the few methods used and is when a film of some liquid or gas completely separates two solids. Fluid lubrication is divided further into hydrostatic, hydrodynamic and elastohydrodynamic lubrication [2,3]. Hydrostatic lubrication is when the fluid film is generated by external systems like pumps, while hydrodynamic lubrication is where the fluid film is self-generated by gathering the fluid under the sliding surface. Elastohydrodynamic lubrication occurs when the pressure in the fluid film is sufficient to deform the solid surfaces. At high contact pressures or low sliding speeds boundary lubrication occurs in which the two surfaces come into contact [4].

Another method that is used to in addition to fluid lubrication is solid lubrication. These are solid materials which exhibit low coefficient of friction and may be preferential to liquid lubrication in select scenarios. A component can be produced from, coated with or made into a composite to give it self-lubricating properties [2,4]. In Chapter 2 and chapter 3, a combination of fluid lubrication and solid lubrication was explored.

1.1 References

[1] Bhushan B. Modern tribology handbook, two volume set. CRC press; 2000.

[2] Ludema KC. Friction, wear, lubrication: a textbook in tribology. CRC press; 1996.

[3] Rabinowicz E. Friction and Wear of Materials, 2nd Edition. Wiley; 1995.

[4] Hutchings IM. Tribology: Friction and Wear of Engineering. Butterworth-Heinemann publications; 1992.

CHAPTER 2 -Tribological behavior of PEEK composites in ethanol and fuel-based lubricants

2.1 Introduction

Polyetheretherketone (PEEK) is a thermoplastic polymer with high mechanical strength, corrosive resistance, and thermal stability. PEEK is semi-crystalline in nature as it has an amorphous phase and a crystalline phase [1]. The crystallinity, which affects the mechanical properties, are affected by the processing temperature, time, and localized cooling rate. Due to its properties, it has found applications in structural components and biomedical devices. In many cases PEEK has been reinforced with additional additives to improve its performance in desired areas. In this case, we are using MAX phase and MAB phase ceramics to improve PEEKs triboactive properties.

MAX, short for $M_{n+1}AX_n$ where n = 1, 2, or 3, phases are ternary ceramics composed of a transition metal (M), p-block elements (A), and either carbon or a nitrogen (X). For comparison, MAB phases are B-containing ternary compounds. These ceramics have a nanolaminate structure which gives them unique properties such as high hardness, thermal stability, and solid lubricating properties [2]. The MAX phase of choice was Cr_2AlC due to its ability to decrease wear rate of PEEK at 10 vol% content under dry sliding conditions while maintaining similar coefficient of friction (μ) to Pure PEEK [3]. Additional lubricants are also used to help improve the tribological conditions with PEEK- MAX/MAB composites.

In this study, F-24 fuel, dodecane, and ethanol were used as low viscosity lubricants. F-24 jet fuel is a kerosene type turbine fuel that conforms to ASTM D1655 and contains Fuel system icing inhibitor (FSII), lubricity improving additive, and static dissipator additive [4]. Dodecane is a major component in kerosene and other jet fuels [5]. Ethanol is a low viscosity alcohol that is produced from renewable resources such as biomass [6].

The main objective of this paper is to study the tribological viability of PEEK matrix composites in high stress, temperature conditions and compatibility in lubricated environments by adding Cr_2AlC or MoAlB to enhance the properties of PEEK.

2.2 Experimental Design

2.2.1 Sample Fabrication

Three compositions were selected for this work; Pure PEEK, PEEK-10vol% Cr_2AlC, and PEEK-10vol% MoAlB, and were fabricated by hot pressing. Commercial PEEK (average particle size 20 μm, Goodfellow Cambridge Limited, Huntingdon, England) was used for a all compositions. Pure samples were fabricated by measuring an amount of PEEK powder that would give the final product a thickness of 4 mm. The powders were pressed in a 1-inch die (MTI) using an Across International cold press at 137.9 MPa for 30 s, twice. The die was then transferred from the cold press to the MTI OTF-1200x hot press. The sample was then pressed in atmospheric air at a heating rate of 10^{o}C/min to 500^{o}C. An initial stress of 14.67 MPa was applied to the sample and maintained during the heating to 500^{o}C. Once at 500^{o}C, the conditions were held for 5 min, and then pressed at a uniaxial stress of 117.4 MPa for 5 min. The sample was cooled to room temperature and removed from the die.

PEEK-MAX or MAB composites were fabricated by measuring out appropriate amounts of PEEK powder and Cr_2AlC or MoAlB powder (< 45 μm) to result in PEEK-10vol% MAX or MAB

phase composites. PEEK powders and MAX or MAB powders were mixed for 5 min using 2 PMMA (polymethyl methacrylate) balls in a ball mill (Model8000 M mixer Mill, SPEX Sample Prep, Metuchen, NJ). The samples were fabricated using the same method mentioned above.

2.2.2 Microstructure, EDS, Wear Scar Analysis

Microstructure and EDS analyses were performed on polished samples. The samples were polished to about 1 μm surface roughness which was measured by averaging 3 readings from a surface profilometer (Surfcom 480A, Tokyo Seimitsu Co. Ltd., Japan).

Secondary electron (SE) and back scattered electron (BSE) images were obtained using a JEOL JSM-6490LV scanning electron microscope (JEOL USA, Inc., Peabody, Massachusetts). SEM images were captured at 500x and 2000x magnification at 15 kV. Wear track EDS images were captured in BSE mode at 500x or 2000x magnification depending on the size of the wear scar.

2.2.3 Tribological Studies

Tribological analysis was done using a tribometer (CSM Instruments SA, Peseux, Switzerland) with a ball on disk method. Dry and lubricated (Ethanol, F-24 fuel, Dodecane) studies were conducted. Lubricated experiments were conducted utilizing a NE-1000 programmable syringe pump (New Era Syringe Pumps Inc., Farmingdale, New York) to apply lubricant at a constant rate of 0.5 mL/min to the surface of the sample during the test (Figure 2.1). 6 mm diameter alumina balls were used as the counterface against Pure PEEK and PEEK MAX or MAB composites. Three replicate experiments measuring coefficient of friction were conducted by using 31.4 cm/s linear speed, 10 mm track radius, and a sliding distance of 500 m. During testing with F-24 fuel lubrication at 20 N had five replicate experiments performed instead of three. We will discuss the rationale behind it in the Results and Discussion section.

The applied load for dry sliding was 20 N. Ethanol lubricated experiments had an applied load of 5, 10, and 20 N whereas F-24 fuel and dodecane only used a 20 N load. The mass of the sample was measured before the experiment and measured after the experiment ended using a weighing scale (Model XA82/220/2X, Radwag Balances and Scales, Poland). Lubricated samples were dried at 100^{o}C in a box furnace (insert model) for 24 hours before the mass is measured for the final time.

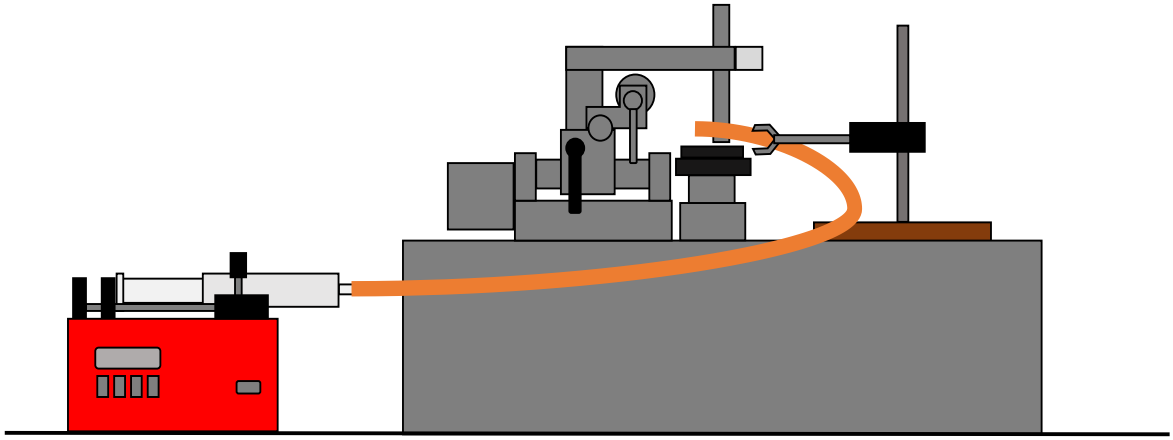

Figure 2.1 Schematics of fluid delivery system for tribology study by using a syringe pump.

The specific wear rate (mm^3/N*m) in equation 1. was determined by dividing the initial mass (m_i) and final mass (m_f) measured in g, by the density of the material (ρ_{th}) and then multiplying by 1000 (volume was converted from cm^3 to mm^3) to find the initial volume and the final volume. The change in volume is calculated by subtracting the final volume from the initial volume. The change in volume is then normalized by dividing it by the product of applied load (N) and sliding distance (d).

$$WR = \left(\frac{m_i}{\rho_{th}} - \frac{m_f}{\rho_{th}}\right)/(N * d) \quad \text{.....1}$$

2.3 Results and Discussion

2.3.1 Microstructure

SE and BSE images of Pure PEEK, PEEK-10% Cr_2AlC, and PEEK-10% MoAlB are shown in Fig. 2.2. Cr_2AlC was randomly spread throughout the matrix as can be seen in Figs. 2.2c and 2.2d as compared to the MoAlB additions where these particles segregated to the phase boundaries to form PEEK-rich surrounded by micro network of PEEK and MoAlB (Figs. 2.2e and 2.2f)

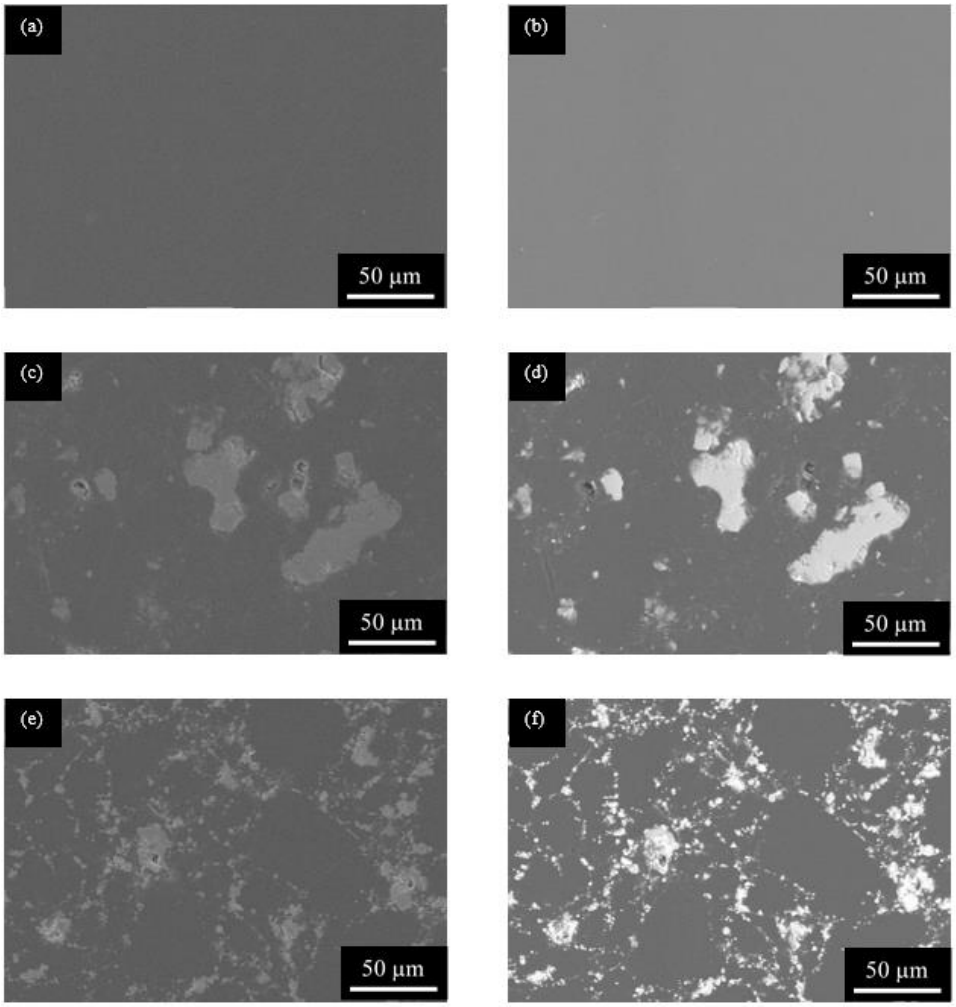

Figure 2.2 Microstructure: SEM SE image of: (a) Pure PEEK, (b) BSE image of the same region, (c) PEEK-10% Cr2AlC, (d) BSE image of the same region, (e) PEEK-10% MoAlB, (f) BSE image of the same region.

2.3.2 Friction

The dry sliding coefficient of friction (μ) under 20 N load is shown in Fig. 2.3. As seen in Fig. 2.3a, Pure PEEK was not able to complete the 500 m cycle. We will discuss the mechanism on the next section. The dry μ of PEEK-10% Cr_2AlC and PEEK-10% MoAlB are shown in Figs. 2.3b and 2.3c, respectively. Plot of the averaged μ of the three compositions are shown in Fig. 2.3d. Pure PEEK had the lowest average friction (~ 0.24) followed by PEEK-10% MoAlB (~ 0.28) and the PEEK-10% Cr_2AlC (~ 0.30). The three compositions primarily display an initial run-in period where the friction is initially low then increases sharply until it flattens out, where the friction slowly increases until the end of the experiment.

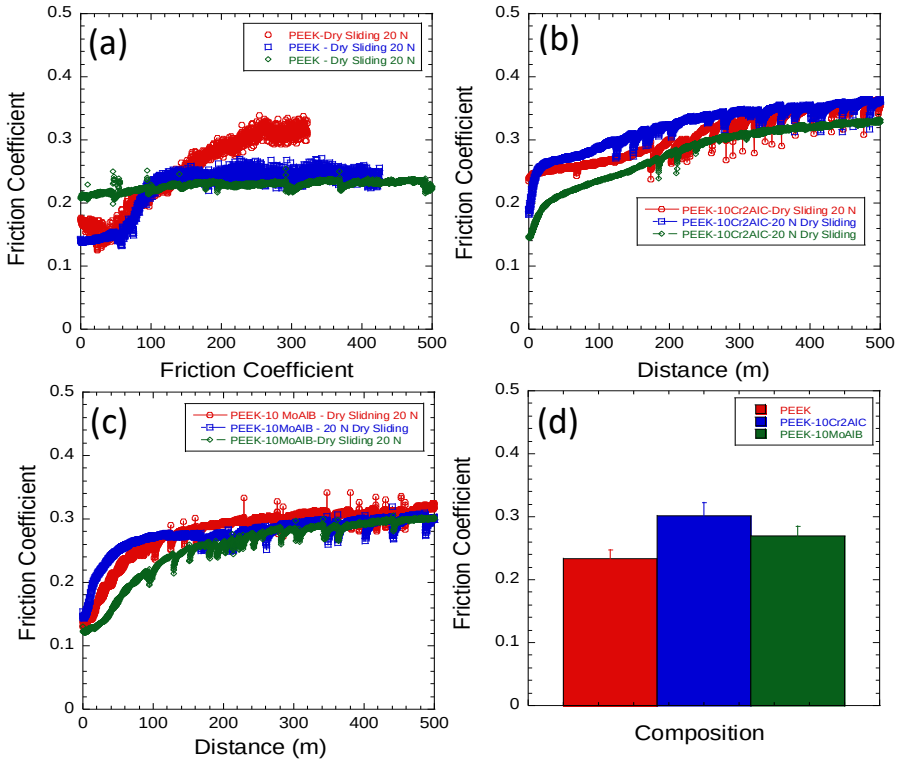

Figure 2.3 Plot of Coefficient of friction (μ) versus distance of, (a) Pure PEEK, (b) PEEK – 10% Cr_2AlC, (c) PEEK – 10% MoAlB, and (d) Average μ of 3 substrates with dry sliding conditions.

Figures 2.4, 2.5, and 2.6 show the μ under ethanol lubrication under 5, 10, and 20 N load, respectively. Figure 2.4 shows that pure PEEK had μ of ~ 0.062 under a 5 N load and ethanol lubrication as compared to PEEK-10% Cr_2AlC which had μ of ~ 0.06 and PEEK- 10% MoAlB had μ of ~ 0.04. In addition, the addition of Cr2AlC and MoAlB had a stabilizing effect on the friction coefficient compered to PEEK which showed the most variability (Fig. 2.4D).

After testing at 10 N in ethanol lubrication, PEEK-10% Cr_2AlC displayed the lowest standard deviation and averaged μ (~ 0.042) as compared to PEEK-10% MoAlB which had the highest standard deviation and average μ (~ 0.078). Pure PEEK was the median in both standard deviation and average μ (~ 0.059) (Fig. 2.5). Comparatively, pure PEEK averaged μ of ~ 0.045 at 20 N and ethanol lubrication followed by PEEK-10% MoAlB (~ 0.05) whereas PEEK-10% Cr_2AlC showed the lowest average μ (Fig. 2.6).

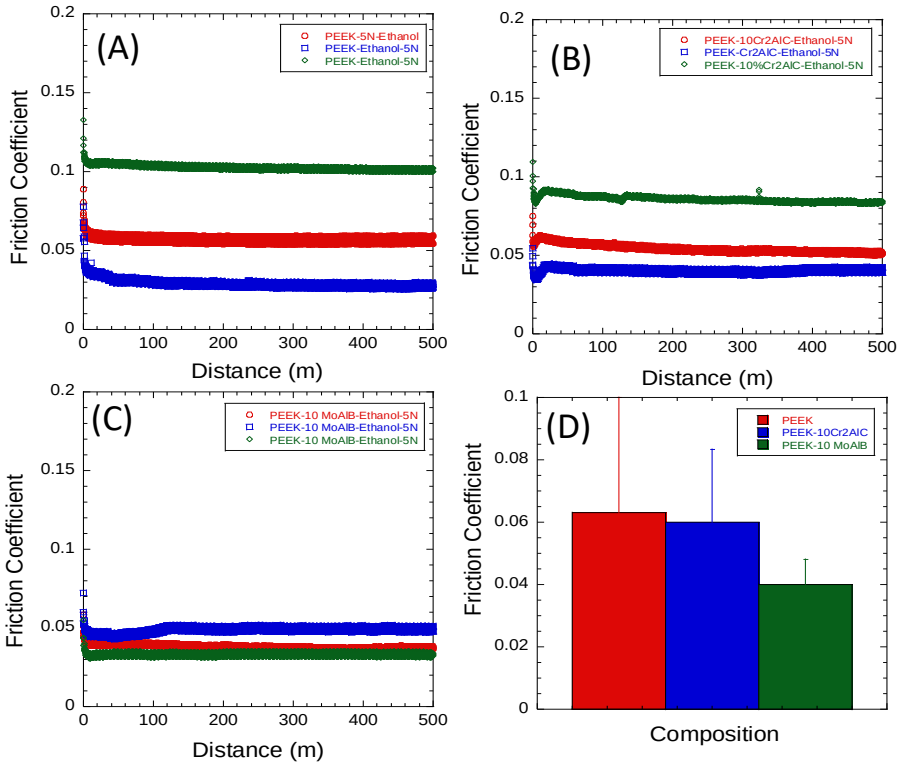

Figure 2.4 Coefficient of friction (μ) of A) Pure PEEK, B) PEEK – 10% Cr_2AlC, C) PEEK – 10% MoAlB, D) Average μ of 3 substrates with Ethanol Lubrication and 5 N load.

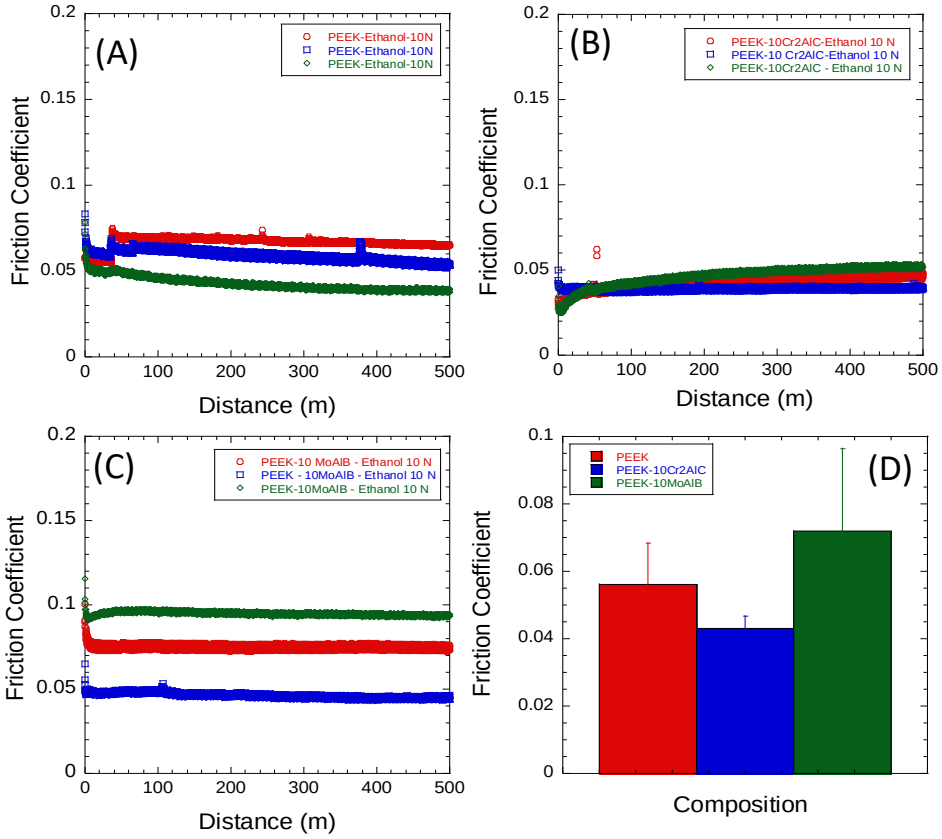

Figure 2.5 Coefficient of friction (μ) of A) Pure PEEK, B) PEEK – 10% Cr_2AlC, C) PEEK – 10% MoAlB, D) Average μ of 3 substrates with Ethanol Lubrication and 10 N load.

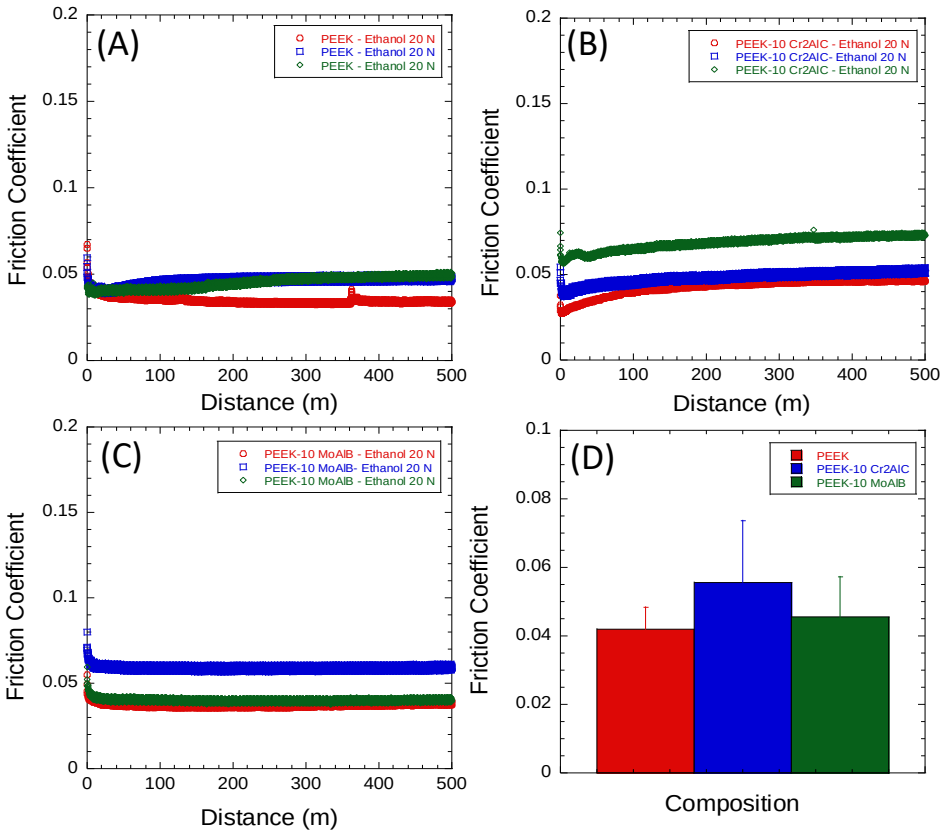

Figure 2.6 Coefficient of friction (μ) of A) Pure PEEK, B) PEEK – 10% Cr_2AlC, C) PEEK – 10% MoAlB, D) Average μ of 3 substrates with Ethanol Lubrication and 20 N load.

Figure 2.7 shows the μ of dodecane lubricated experiments at 20 N load. PEEK had the lowest average μ (~ 0.04) at these conditions but had the largest standard deviation. Cr_2AlC and MoAlB stabilized the friction and decreased the standard deviation between replicates. PEEK-10% MoAlB had the averaged μ of ~ 0.045 and PEEK-10% Cr_2AlC had the largest μ at ~ 0.05.

As discussed earlier, tribology experiments showing the μ on pure PEEK, PEEK-10% Cr_2AlC, and PEEK-10% MoAlB using a 20 N load and F-24 fuel lubrication (Fig. 2.8) had five replicate experiments performed instead of three as the results showed high variability. A replicate experiment of pure PEEK showed a large increase in friction from ~ 0.05 to ~ 0.14 (Fig. 2.8a) which, may have been an indication of scuffing behavior. The addition of Cr_2AlC slightly

increased the average μ (~ 0.075) compared to pure PEEK (~ 0.05). The addition of MoAlB also showed an increase in average μ (~ 0.06) compared to pure PEEK (~ 0.05).

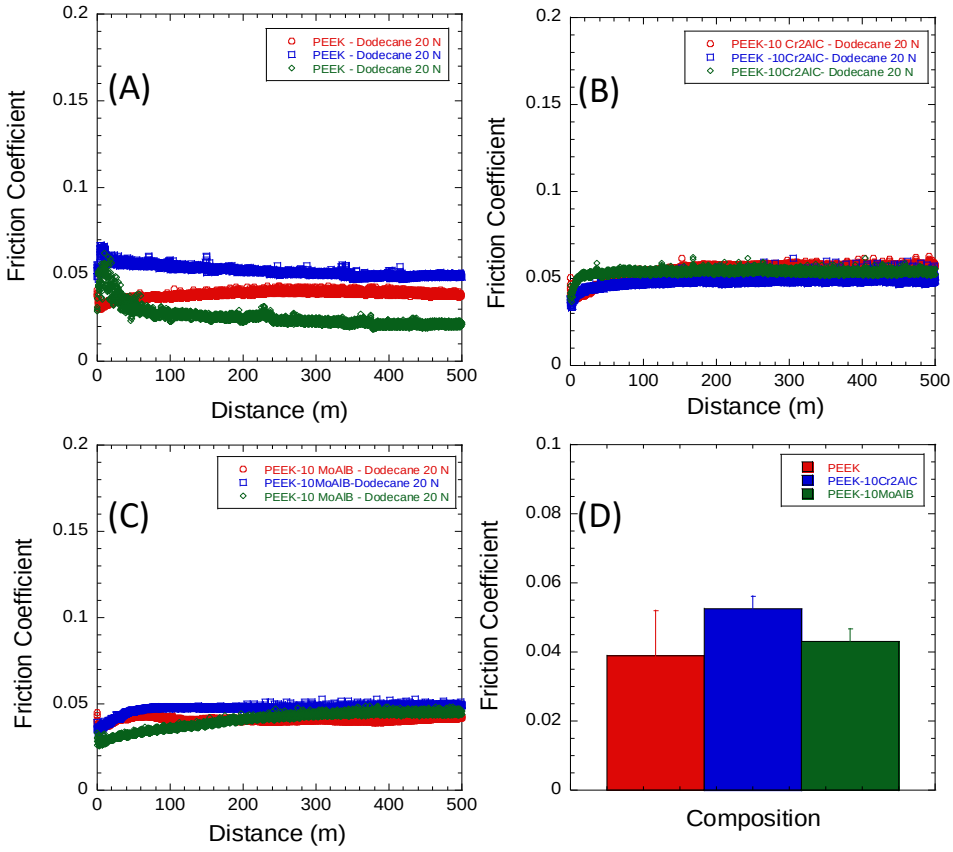

Figure 2.7 Coefficient of friction (μ) of A) Pure PEEK, B) PEEK – 10% Cr_2AlC, C) PEEK – 10% MoAlB, D) Average μ of 3 substrates with dodecane Lubrication and 20 N load.

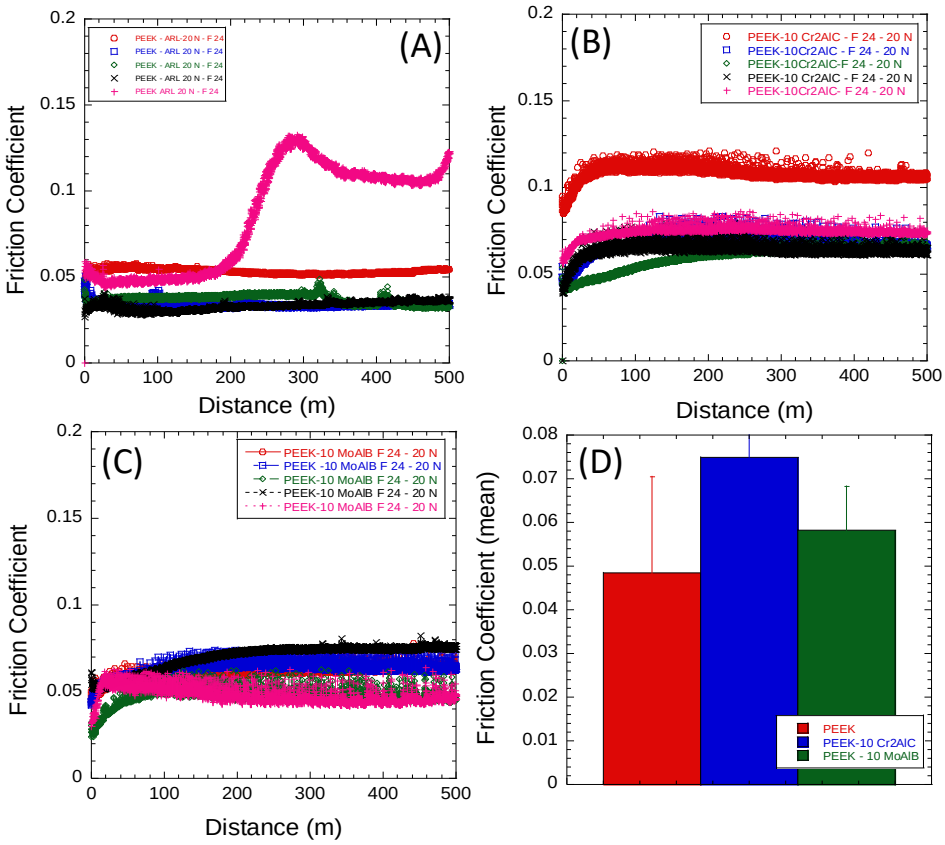

Figure 2.8 Coefficient of friction (μ) of A) Pure PEEK, B) PEEK – 10% Cr_2AlC, C) PEEK – 10% MoAlB, D) Average μ of 3 substrates with F-24 fuel Lubrication and 20 N load

2.3.3 Wear Rate

The specific wear rates of all compositions and specific conditions are given in Figure 2.9. Samples lubricated by ethanol showed lower wear rates at 20 N than those lubricated by F-24 fuel and dodecane as well as during dry sliding. The wear rate of ethanol lubricated PEEK-10% MoAlB decreased as load increased from 5 to 10 to 20 N and was the lowest overall wear rate by using ethanol at 20 N load. Ethanol lubricated pure PEEK samples showed the lowest wear at 5 and 10 N compared to PEEK-10% Cr_2AlC and PEEK-10% MoAlB using the same conditions. F-24 and dodecane lubricated samples showed comparable wear rates at 20 N. Pure PEEK displayed the highest wear during dry sliding at 20 N. PEEK-10% Cr_2AlC during dry sliding at 20 N had

comparable wear rate to PEEK-10% Cr_2AlC and PEEK-10% MoAlB under ethanol lubrication and 10 N load.

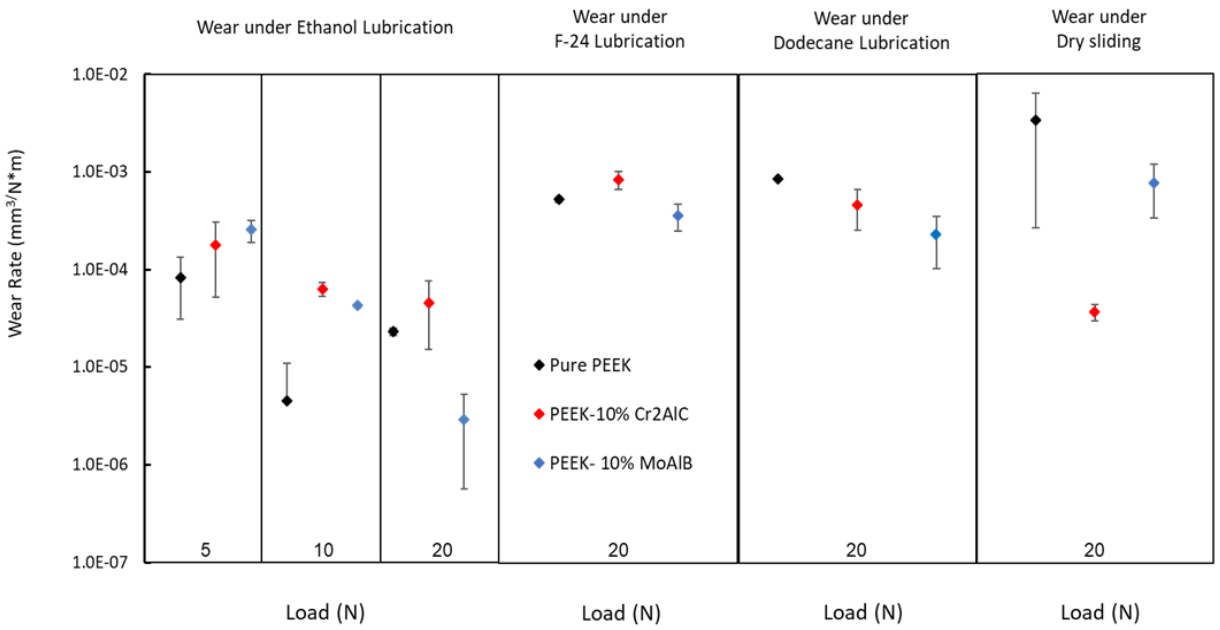

Figure 2.9 Calculated wear rate of Pure PEEK, PEEK – 10% Cr_2AlC, and PEEK – 10% MoAlB due to load and lubrication method

2.3.4 Wear Scars Analysis

SEM and EDS analysis were performed on the wear scars of the pure PEEK, PEEK-10% Cr_2AlC, PEEK-10% MoAlB and alumina balls. BSE images in Figure 2.10 show points of interest on the various substrates and their counterfaces that were used for dry sliding analysis at 20 N load. Wear was observed in Fig. 2.10a, as the formation of transfer film and PEEK debris (point A1' and A2' in Table 2.1 respectively) can be seen on the alumina counterface. Abrasive wear was observed between PEEK-10% Cr_2AlC and Alumina (Fig. 2.10c). Wear debris can be seen on the surface of the substrate and the formation of oxides at point B2 are shown in Table 2.1. Long striations were formed on the alumina counterface due to the MAX phase reinforcements in PEEK and small amounts of it were detected on the alumina's surface at point B1'. The abrasive wear of

PEEK-10% MoAlB is seen in figure 2.10e. The surface structure has been changed due to the wear as the MoAlB along the grain boundaries that was seen clearly in the original microstructure (Figure 2.1) were no longer observable.

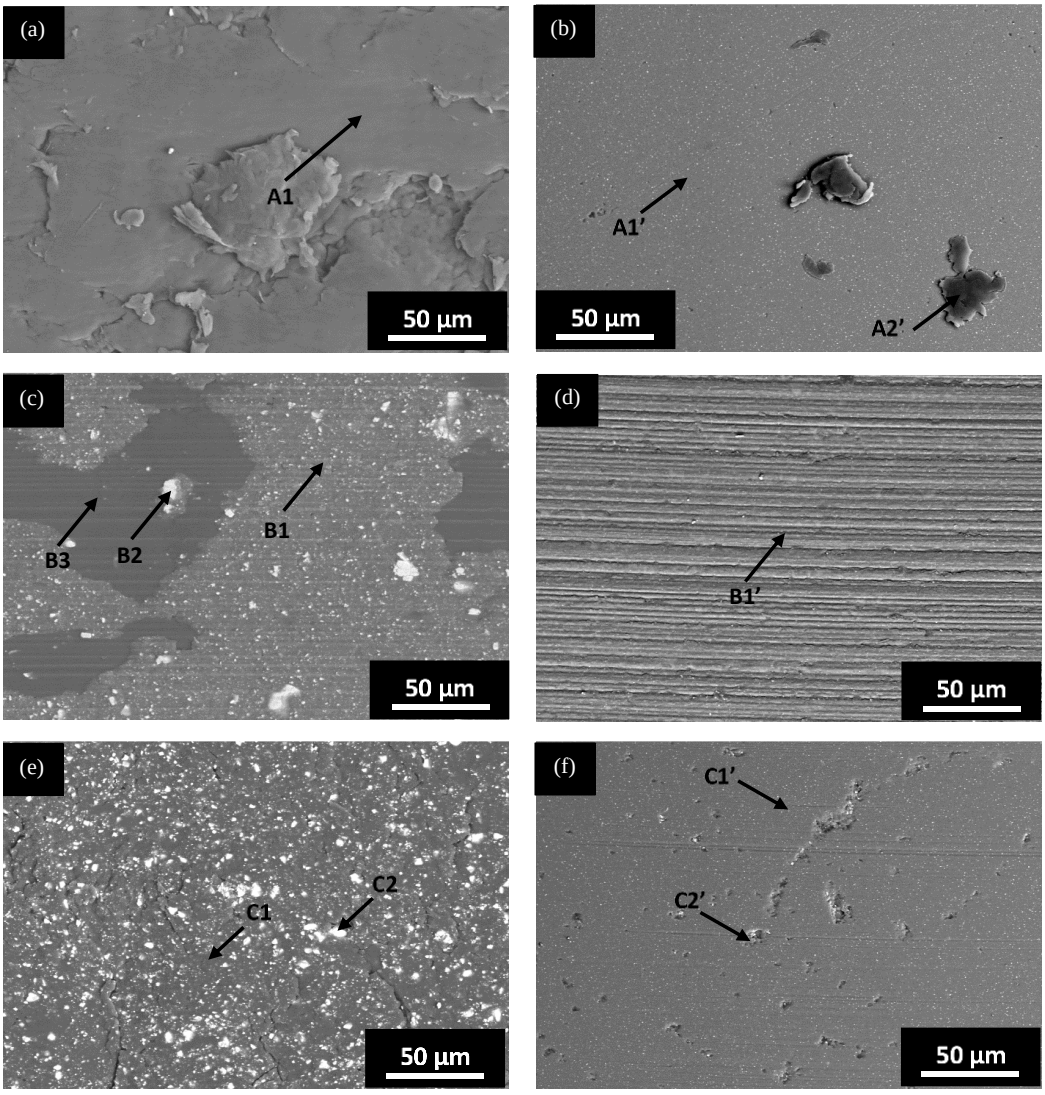

Figure 2.10 EDS of Dry sliding at 20 N load a) wear track of Pure PEEK, b) Alumina bearing counterface used on Pure PEEK, c) wear track of PEEK-10% Cr_2AlC, d) Alumina bearing counterface used on PEEK-10% Cr_2AlC, e) wear track of PEEK-10% MoAlB, f) Alumina bearing counterface used on PEEK-10% MoAlB

Material	Notes	Points	C	O	Al	Cr	Mo	B
Pure PEEK	20 N load, dry sliding	A1	100±1.62	x	x	x	x	x
Alumina ball	20 N load, dry sliding	A1'	5.69±0.98	46.92±1.08	47.39±0.63	x	x	x
		A2'	92.87±1.62	x	7.13±0.25			
PEEK-10%Cr2AlC	20 N load, dry sliding	B1	62.76±1.17	26.26±1.35	4.18±0.20	6.80±0.44	x	x
		B2	13.91±0.79	51.18±2.86	32.44±0.45	3.48±0.28		
		B3	99.40±1.51	x	x	0.60±0.20		
Alumina ball	20 N load, dry sliding	B1'	8.20±0.89	39.42±3.57	49.02±0.68	3.36±0.36	x	x
PEEK-10% MoAlB	20 N load, Dry sliding	C1	97.23±2.46	x	1.53±0.14	x	1.24±0.18	x
		C2	46.90±4.90		26.09±0.48		27.00±0.67	
Alumina ball	20 N load, Dry sliding	C1'	6.64±0.90	47.30±1.03	46.05±0.60	x	x	x
		C2'	13.98±1.11	41.30±1.31	44.72±0.67			

Table 2.1 EDS results of PEEK and PEEK-composites due to dry sliding

The SEM and EDS ethanol lubricated wear scars are shown in Figure 2.11. Minor wear can be observed on pure PEEK (Fig. 2.11a) and transfer film was formed on the alumina surface (Fig. 2.11b). PEEK-10% Cr_2AlC displayed wear behavior and the formation of a transfer film was observed on the alumina counterface. This is confirmed by point E2' in Table 2.2 that shows mostly PEEK with a small amount of Cr indicating the presence of Cr_2AlC on the surface (Fig. 2.11 d). PEEK-10% MoAlB also showed similar wear and transfer film was observed on the alumina surface (Figs. 2.11 e-f). The formation of stable tribofilms can account for the enhanced tribological behavior of PEEK and PEEK-based composites during ethanol lubrication. Currently, we are performing spectroscopic studies to understand the tribochemistry of these tribofilms.

Wear scars of dodecane lubricated (20 N load) samples are given in Fig. 2.12. Pure PEEK under dodecane lubrication displayed wear (G2, Table 2.3). Low amounts of PEEK were detected at both points G1' and G2' (Table 3) on the alumina counterface in Fig. 2.12b. Abrasive wear was observed on both PEEK-10 Cr_2AlC and PEEK-10% MoAlB and their respective counterfaces. A transfer film occurred on the alumina counterface of PEEK-10% Cr_2AlC. As compared to

tribosurfaces obtained after ethanol lubrication, the tribosurfaces showed significant damage and stable tribofilm was not observed which can account for the poor tribological performance in dodecane. Comparatively, Fig. 2.13 and Table 2.4 show the tribosurfaces after F-24 lubrication. After F-24 lubrication all the samples showed significant damage. In other words, no transfer film was observed unlike ethanol-based lubrication.

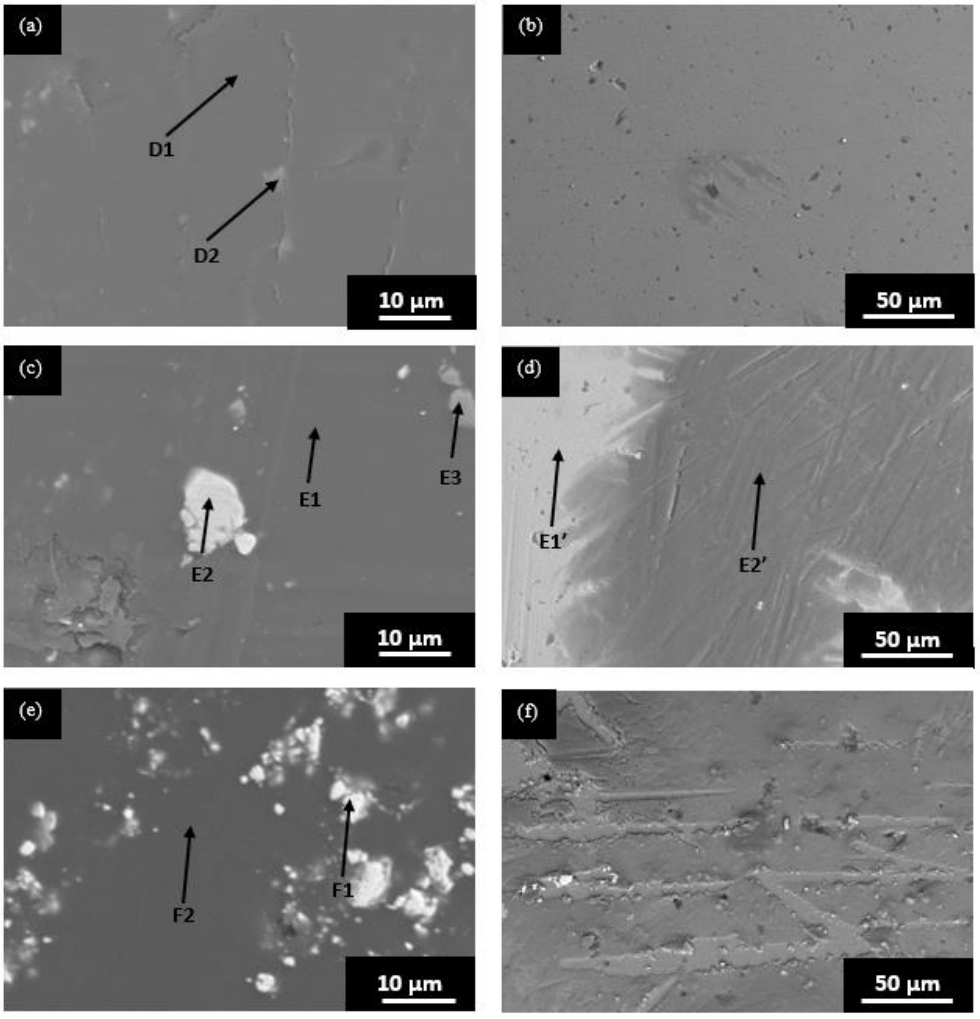

Figure 2.11 EDS of Ethanol Lubricated at 20 N load a) wear track of Pure PEEK, b) Alumina bearing counterface used on Pure PEEK, c) wear track of PEEK-10% Cr_2AlC, d) Alumina bearing counterface used on PEEK-10% Cr_2AlC, e) wear track of PEEK-10% MoAlB, f) Alumina bearing counterface used on PEEK-10% MoAlB

Material	Notes	Points	C	O	Al	Cr	Mo	B
Pure PEEK	20 N load, Ethanol lubrication	D1	100±1.61	x	x	x	x	x
		D2	64.88±1.25	35.12±2.31				
PEEK-10%Cr2AlC	20 N load, Ethanol lubrication	E1	100±1.62	x	x	x	x	x
		E2	13.49±0.88	5.20±1.24	27.50±0.62	53.81±1.28		
		E3	78.08±3.99	13.74±7.18	x	8.17±2.34		
Alumina ball	20 N load, Ethanol lubrication	E1'	9.29±1.13	39.95±4.31	50.74±0.72	0.02±0.11	x	x
		E2'	86.77±2.20	6.81±1.87	7.01±0.49	0.40±0.37		
PEEK-10% MoAlB	20 N load, Ethanol lubrication	F1	13.35±1.92	x	37.60±0.89	x	49.05±1.28	x
		F2	100±1.63		x		x	

Table 2.2 EDS Results of PEEK and PEEK-composites due to Ethanol Lubrication

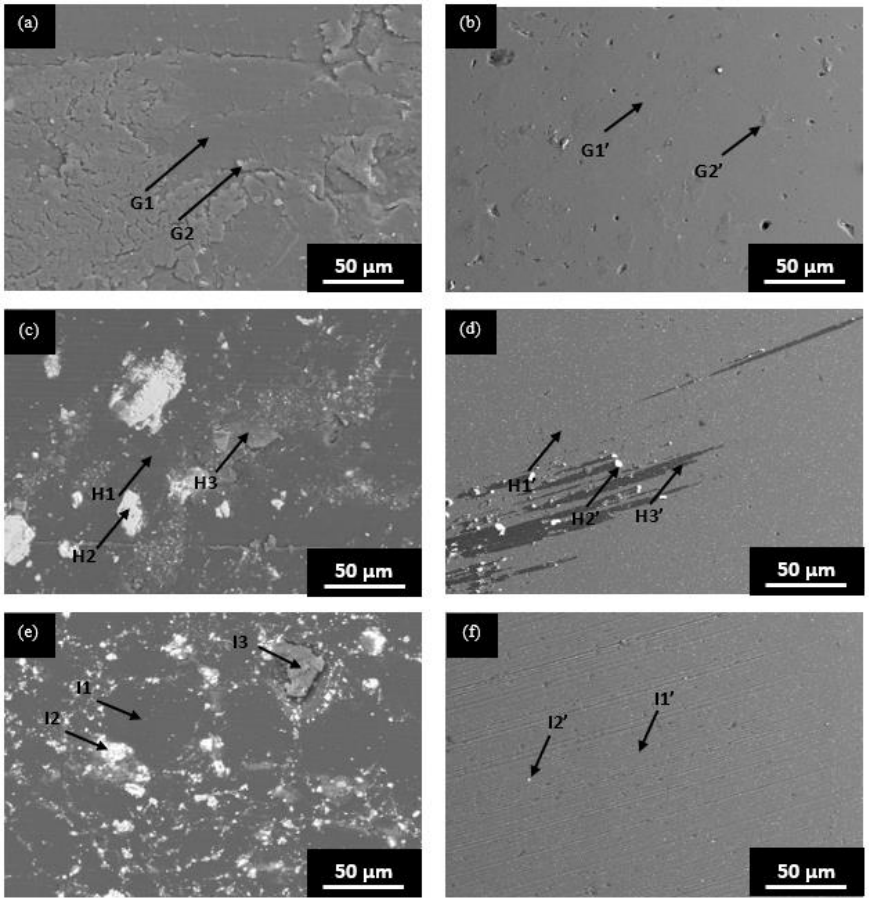

Figure 2.12 EDS of dodecane Lubricated at 20 N load a) wear track of Pure PEEK, b) Alumina bearing counterface used on Pure PEEK, c) wear track of PEEK-10% Cr_2AlC, d) Alumina bearing counterface used on PEEK-10% Cr_2AlC, e) wear track of PEEK-10% MoAlB, f) Alumina bearing counterface used on PEEK-10% MoAlB

Material	Notes	Points	C	O	Al	Cr	Mo	B
Pure PEEK	20 N load, Dodecane lubrication	G1	100±1.69	x	x	x	x	x
		G2	90.16±1.48	9.50±0.64	0.34±0.13			
Alumina ball	20 N load, Dodecane lubrication	G1'	4.88±1.18	53.04±1.54	42.09±0.72	x	x	x
		G2'	13.46±1.99	52.78±2.15	33.76±0.81			
PEEK-10%Cr2AlC	20 N load, Dodecane lubrication	H1	99.34±1.57	x	0.05±0.04	0.61±0.22	x	x
		H2	14.20±0.55		27.91±0.61	57.89±1.27		
		H3	52.97±1.33	36.83±1.91	5.93±0.34	4.27±0.53		
Alumina ball	20 N load, Dodecane lubrication	H1'	7.33±1.41	49.73±1.62	42.94±0.76	x	x	x
		H2'	8.62±1.61	47.76±1.82	43.62±0.84			
		H3'	6.05±1.04	53.18±1.64	40.77±0.74			
PEEK-10% MoAlB	20 N load, Dodecane lubrication	I1	100±1.64	x	x	x	x	x
		I2	16.28±1.71	17.64±2.19	31.31±0.63		27.67±0.76	7.10±4.94
		I3	52.13±3.31	36.56±1.77	7.11±0.25		4.20±0.31	x
Alumina ball	20 N load, Dodecane lubrication	I1'	10.65±1.67	48.08±2.14	41.26±0.94	x	x	x
		I2'	9.97±1.67	49.12±2.09	40.91±0.91			

Table 2.3 EDS Results of PEEK and PEEK-composites due to dodecane Lubrication

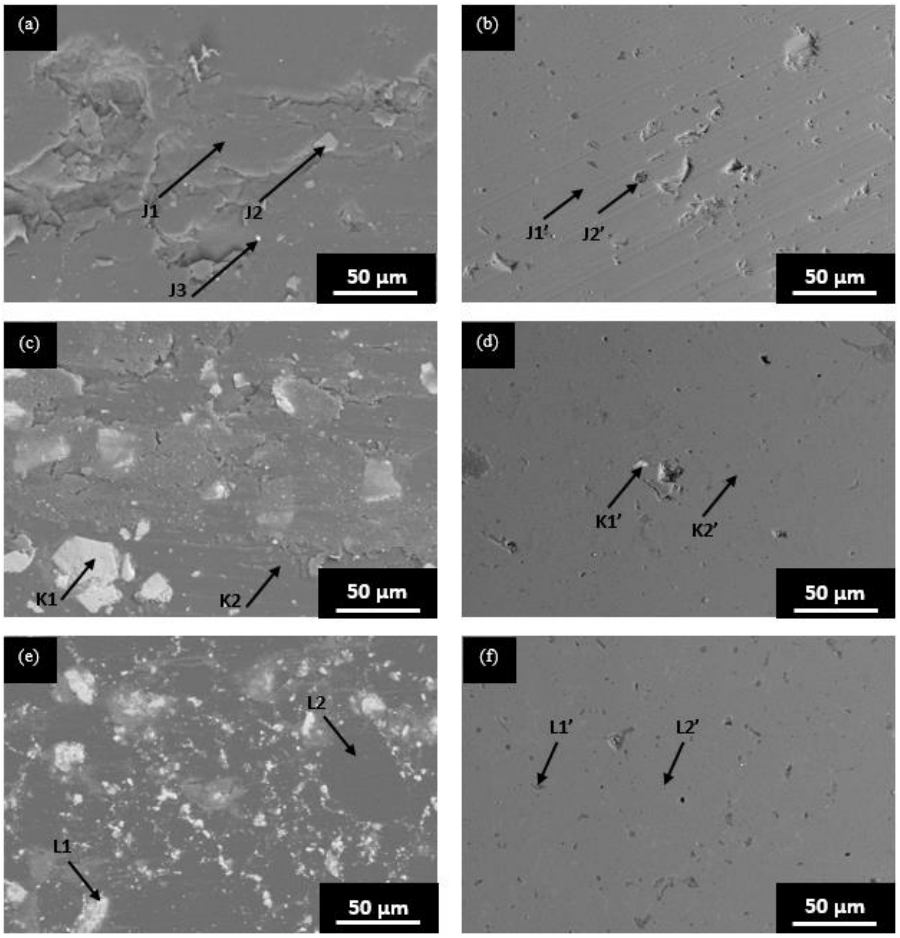

Figure 2.13 EDS of F-24 Lubricated at 20 N load a) wear track of Pure PEEK, b) Alumina bearing counterface used on Pure PEEK, c) wear track of PEEK-10% Cr_2AlC, d) Alumina bearing counterface used on PEEK-10% Cr_2AlC, e) wear track of PEEK-10% MoAlB, f) Alumina bearing counterface used on PEEK-10% MoAlB

Material	Notes	Points	C	O	Al	Cr	Mo	B
Pure PEEK	20 N load, F-24 lubrication	J1	73.31±1.34	26.61±2.18	0.08±0.04	x	x	x
		J2	97.08±5.23	x	2.92±0.37			
		J3	74.42±2.61	22.15±2.02	2.16±0.23		1.27±0.21	
Alumina ball	20 N load, F-24 lubrication	J1'	6.69±1.24	45.71±1.20	47.60±0.67	x	x	x
		J2'	14.07±3.07	53.43±1.12	32.51±0.45			
PEEK-10%Cr2AlC	20 N load, F-24 lubrication	K1	12.65±0.94	x	28.28±0.69	59.07±1.48	x	x
		K2	73.75±1.39	24.32±2.42	0.82±0.17	1.11±0.38		
Alumina ball	20 N load, F-24 lubrication	K1'	33.08±2.74	25.09±3.40	28.38±0.95	12.88±1.13	x	x
		K2'	11.26±1.32	46.54±3.40	42.39±0.61	x		
PEEK-10% MoAlB	20 N load, F-24 lubrication	L1	24.80±1.38	13.95±1.93	29.16±0.57	x	24.84±0.74	7.26±2.27
		L2	100±1.63	x	x		x	x
Alumina ball	20 N load, F-24 lubrication	L1'	12.79±1.80	23.66±1.40	58.46±0.93	x	0.14±0.40	4.95±6.43
		L2'	19.31±3.14	11.95±1.87	64.08±1.18		0.26±0.44	4.40±16.11

Table 2.4 EDS Results of PEEK and PEEK-composites due to F-24 Fuel Lubrication

2.4 Conclusions

In this Chapter, different types of PEEK-based composites were synthesized by Cr_2AlC and MoAlB additions. The addition of these phases improved the wear performance of PEEK-based composites during dry sliding. During lubrication with ethanol, all the compositions showed lower wear than dry sliding. Detailed inspection of wear tracks showed the formation of stable tribofilms which can account for the better tribological behavior. Comparatively, all the compositions showed high wear in F-24 and dodecane lubrication as compared to ethanol lubrication. Detailed inspection of the wear tracks showed the formation of wear tracks and absence of a stable tribofilm which can explain this behavior.

2.5 References

[1] Kurtz SM, Devine JN. PEEK biomaterials in trauma, orthopedic, and spinal implants. Biomaterials. 2007;28(32):4845-4869.

[2] Barsoum MW. The MN+ 1AXN phases: A new class of solids: Thermodynamically stable nanolaminates. Progress in solid state chemistry. 2000;28(1-4):201-281

[3] Javaid S, Dey M, Kaabouch N, Gupta S. On the potential of polyetheretherketone matrix composites reinforced with ternary nanolaminates for tribological and biomedical applications. Journal of applied polymer science. 2021;138(10):49980.

[4] Federal Aviation Administration, Special Airworthiness Information Bulletin, SAIB NE-14-28, 2014

[5] Moldoveanu SC. Pyrolysis of organic molecules. InApplications to Health and Environmental Issues 2019. Elsevier.

[6] Ramadhas AS. Alternative fuels for transportation. Taylor & Francis; 2011.

CHAPTER 3 - Evaluation of tribological behavior of SiC and Si_3N_4 under different tribological conditions

3.1 Introduction

Advanced ceramics like silicon carbide (SiC) and silicon nitride (Si_3N_4) are important materials for structural applications due to their high hardness, low density, refractoriness, and chemical resistance [1-6]. SiC ceramics have potential in structural components like bearings, seals, nozzles, cutting tools, heat exchangers and turbine parts etc [2]. Silicon nitride also has potential in different applications like heat exchangers, turbine and automotive engine components with refractoriness, engine valves and tribological components [5, 6].

Sustainable, energy-efficient components coupled with reduction in emissions have become integral component of research in designing next generation machines. A key push towards this vision is the replacement of metal-oil tribosystems with water-based or sustainable systems like ethanol [2, 7]. Advanced ceramics like Si_3N_4 and SiC are playing pivotal roles in water-based lubrication systems [2, 3]. Both Si_3N_4 and SiC have shown strong potential for water-based lubricated system. Chen et al. [3] had reported that Si_3N_4 has larger load carrying capacity than SiC. Zhang et al. [2] had summarized after literature survey that self-mated SiC can have low friction over wider spectrum of sliding velocity and are resistant to abrasive wear. Comparatively, oxide ceramics are prone to water accelerated crack growth [2].

The goal of this study is to study the tribological behavior of commercially available SiC (Hexoloy) and Si_3N_4 (NT-154, SN-281, and AS-800).

3.2 Experimental Design

3.2.1 Fabrication

Commercial grade SiC (Hexoloy-SA, Saint Gobain) and Si_3N_4 (NT-154, SN-281, and AS-800) were used during this study. Hexoloy® SA SiC is sintered alpha silicon carbide (without pressure) and has >98% theoretical density with a grain structure in the range of 4-10 microns. It does not contain any free Si [9]. Saint Gobain NT-154 has Y_2O_3 as the sintering additive [8]. SN-281 was obtained from Kyocera America, WA and has about 9–10 wt.% Lu_2O_3 as a sintering additive [6]. Honeywell AS-800 is manufactured by using Y_2O_3, La_2O_3, and SrO as sintering aids [8, 10]. The Hexoloy specimen were cut into 2.5 cm x 2.5 cm x 0.4 cm prismatic samples. NT-154, SN-281, and AS-800 had dimensions of ~1.27 cm x ~1.27 cm x ~0.4 cm. Samples were polished to ~1 μm surface roughness.

3.2.2 Tribology

Tribology experiments were conducted by using a CSM instruments tribometer with a pin on disk method. Three replicate experiments measuring coefficient of friction were performed on each composition using a 4 mm wear track ring radius, 500 m sliding distance, 20 cm/s linear speed, an applied load of 5 N and a 6 mm diameter alumina ball as a counter face. Both dry and lubricated experiments were conducted using deionized (DI) water and ethyl alcohol as the lubricants. The lubricants were applied to the samples by using a syringe pump system at a rate of 0.5 mL/min (Fig. 2.1). The wear rate was calculated by measuring the mass of a sample and the alumina ball counter face before the experiment and measuring the mass after the experiment using a high precision weighing scale.

The specific wear rate (WR) ($mm^3/N*m$) is defined in Eq. I where m_i is initial mass and m_f is mass after the tribological process, and ρ_{th} is the density. The change in volume is calculated by

subtracting the final volume from the initial volume. The change in volume is then normalized by dividing it by the product of applied load (N) and sliding distance (d).

$$WR = \left(\frac{m_i}{\rho_{th}} - \frac{m_f}{\rho_{th}}\right)/(N * d) \ldots\ldots\ldots\ldots\ldots\ldots (I)$$

3.2.3 Microstructure, EDS, and Wear track analysis

The microstructure of all samples was captured in secondary electron (SE) and backscattered electron (BSE) mode using a scanning electron microscope (SEM, JEOL JSM-6490LV, JEOL USA, Inc., Peabody, Massachusetts). Chemical analysis was performed using a Thermo Nanotrace energy-dispersive X-ray detector with NSS-300e acquisition in a point analysis mode taking three measurements at each point of interest which are averaged and reported in the following sections. The wear tracks that occurred during the tribology experiments on both the substrate and the counter face were observed under SE and BSE at 500x magnification.

3.3 Results and Discussion

3.3.1 Microstructure and Tribological Behavior

Figure 3.1 shows the dense microstructure of Hexoloy, NT-154, SN-281, and AS-800. Figure 3.2a shows the friction coefficients of Hexoloy against alumina by utilizing different lubricants. In the case of dry sliding of Hexoloy against alumina, the friction coefficient versus distance profile displayed dual stage behavior, where initially, it displayed low friction coefficient and then it increased to higher values as compared to lubrication in water where the friction decreased after the run-in period (Fig. 3.2a). Comparatively, during lubrication with ethanol, the friction coefficient was comparatively lower although signs of fluctuations were observed. Hexoloy had the highest friction coefficient during dry sliding with an average of ~0.34. DI water

showed a minor improvement in friction as it was ~0.27. Ethanol reduced the friction greatly to ~ 0.18 as compared to dry sliding (~53 % reduction) (Fig. 3.2c).

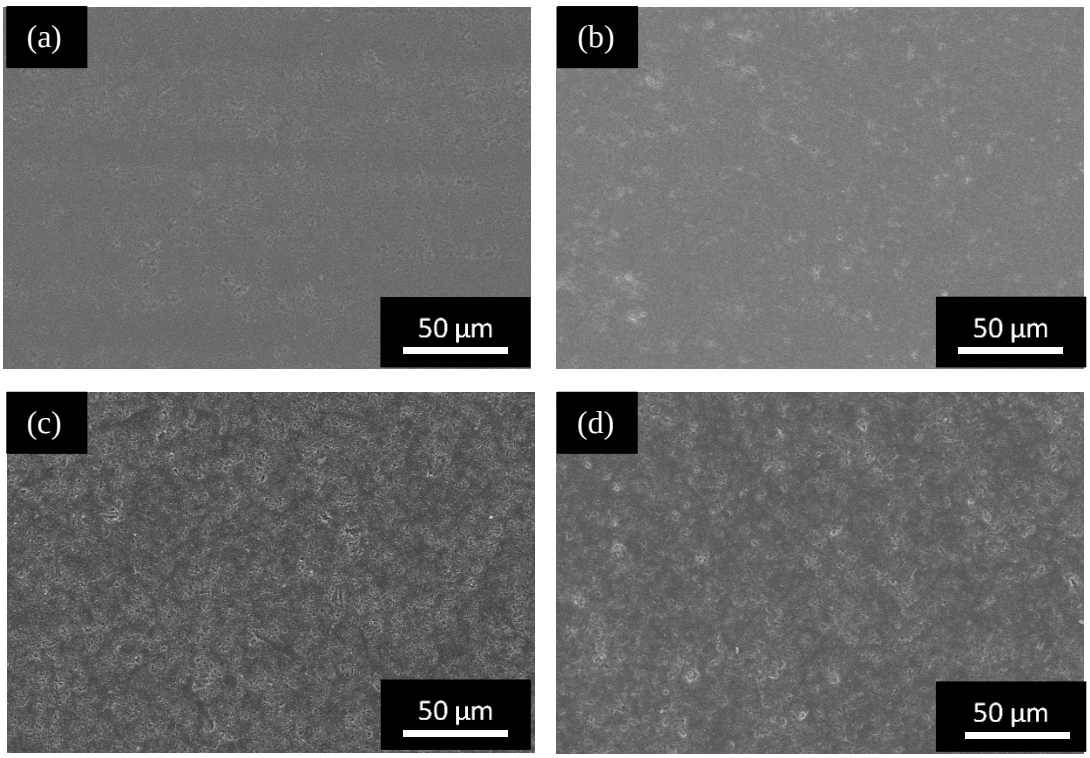

Figure 3.1 Microstructure: SEM SE microstructure of, (a) Hexoloy, (b) NT-154, (c) SN-281, and (d) AS-800.

The total wear in Fig. 3.2b had a similar trend to that of the average friction coefficients where dry sliding had the highest observed wear followed by DI water being the median observed wear, and lastly, ethanol (the wear rate was improved by two-orders of magnitude). These results show that ethanol is a promising lubricant for Hexoloy components.

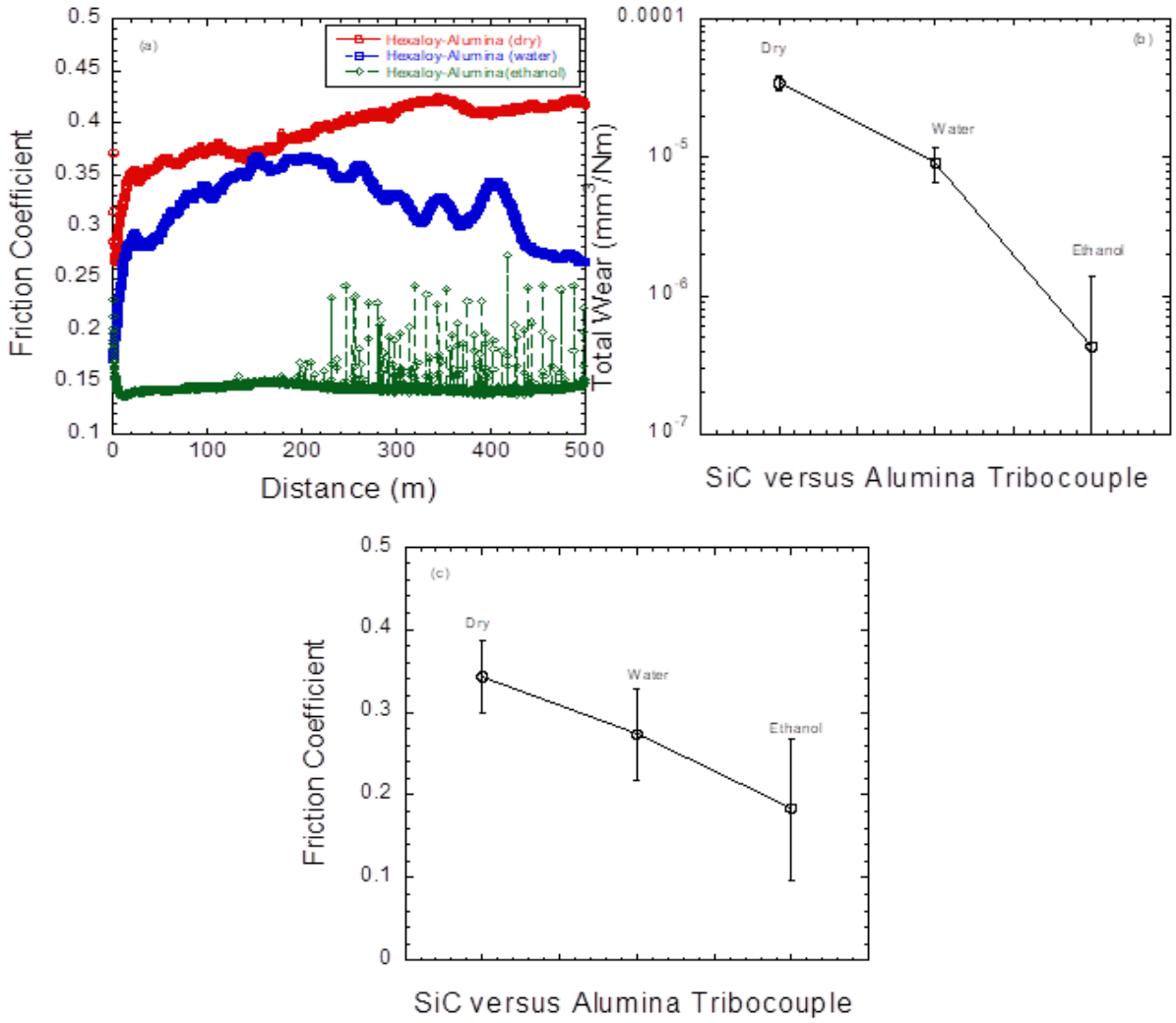

Figure 3.2 Plot of, (a) friction coefficient versus distance, and (b) total wear (c) friction coefficient of SiC versus alumina tribocouples under different conditions.

The friction behavior of NT-154, SN-281, and AS-800 during dry sliding, DI water, and ethanol are compared in Fig. 3.3. DI water and ethanol lubrication decreased the friction of the Si_3N_4 samples as compared to dry sliding. During dry sliding, NT-154 had the lowest observed WR of the dry sliding samples (~1.73 x 10^{-5} mm^3/Nm) while AS-800 had the highest observed WR of ~1.85 x 10^{-4} mm^3/Nm (Fig. 3.4). Comparatively, Hexoloy had a similar WR of ~3.45 x 10^{-5} mm^3/Nm to NT-154 and lower WR than AS-800.

During wear studies in DI water, AS-800 had the lowest wear rate (~1.22 x 10^{-5} mm^3/Nm) as compared to both SN-281 (~6.72 x 10^{-5} mm^3/Nm) and NT-154 (~5.45 x 10^{-5} mm^3/Nm) which had similar wear rate. Comparatively in ethanol, both AS-800 (~1.23 x 10^{-5} mm^3/Nm) and SN-281 (~8.05 x 10^{-6} mm^3/Nm) showed lower wear rate than NT-154 (~4.64 x 10^{-5} mm^3/Nm). These results showed that AS-800 showed superior performance during both DI water and ethanol lubrication. Comparatively, Hexoloy showed WR of ~9.11 x 10^{-6} and ~4.30 x 10^{-7} mm^3/Nm mm^3/Nm in DI water and ethanol, respectively. These results showed the Hexoloy performed better than different grades of Si_3N_4. We will discuss the potential mechanisms in the next section.

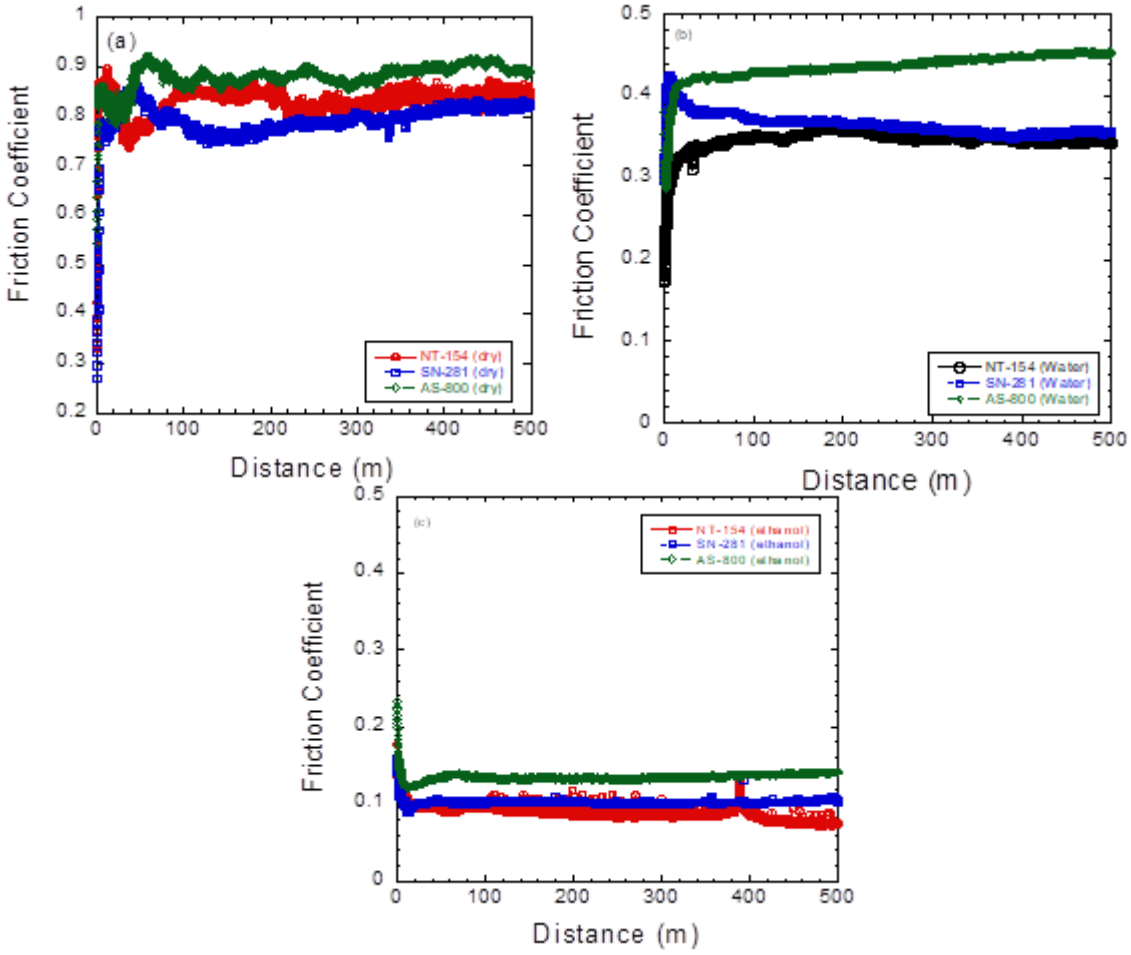

Figure 3.3 Plot of friction coefficient versus distance of different types of Si_3N_4 under, (a) dry, and lubricated by, (b) water and (c) ethanol.

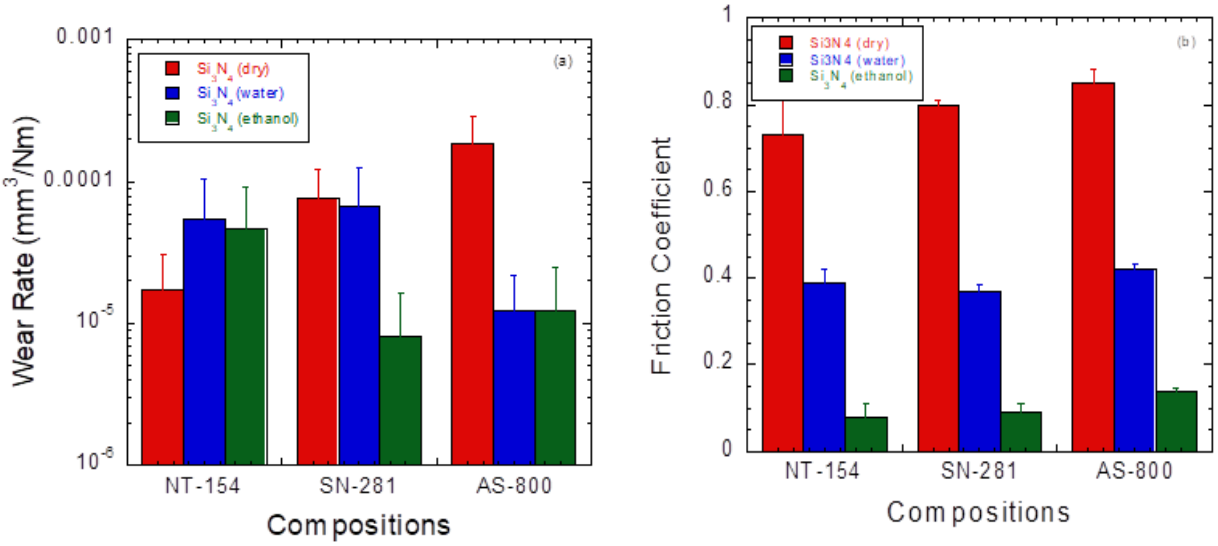

Figure 3.4 Plot of, (a) wear rate and (b) friction coefficient of different Si3N4 compositions under dry and lubricated conditions.

3.3.2 Wear Surface Analysis and Potential Mechanisms

3.3.2.1 Tribology during Dry Sliding

Figure 3.5 presents the wear scars of the samples used for dry sliding experiments. Hexoloy and its corresponding alumina counterface are given in Figs. 5a and 5b, respectively. Both surfaces showed abrasive wear tracks. Oxidation, as well as alumina wear debris, was detected at points A2 and A3 which is further corroborated by the high O/Si ratios in these areas (Table 3.1). SiC wear debris was also detected on the corresponding alumina counterface at point A2' (Table 3.1). The generation of abrasive third body can account for the high wear in Hexoloy. It is well documented in literature that SiC shows dual stage behavior where initially the wear is mild thereafter it transitions into fracture dependent wear thus displaying poor tribological characteristics during dry sliding [12]. This study also showed fracture and third body formation dependent tribological process results in high wear rate in Hexoloy-alumina tribocouples.

Comparatively, Si_3N_4 samples (NT-154, SN-281, and AS-800) also showed abrasive wear track and oxidation (Fig. 3.5 and Table 1). As a background, NT-154 is produced by hot-isostatic pressing where Y_2O_3 is the sintering aid which results in the formation of $Y_2Si_2O_7$ at grain boundaries [8]. NT-154 has a fine grained equiaxed microstructure and low amount of glass phase. It has a fracture toughness of 5.5 to 6.0 MPa·$m^{1/2}$ and room temperature flexural strength in the rage of 900 to 1000 MPa [8]. Comparatively, AS-800 is produced by gas-pressure liquid-phase sintering with La_2O_3, Y_2O_3, and SrO as additives and has an interlocking microstructure with 80% equiaxed (0.5 μm grain size) and 20% acicular (1.5-2 μm grain size) [8]. This composition has a fracture toughness of ~8 MPa·$m^{1/2}$ and flexural strength of ~800 MPa. SN-281 is produced by Hot Isostatic Pressing and the microstructure is composed of mainly equiaxed with grain size in the range of (0.69 ±0.10) μm and small amounts of large grains of length of 30 μm and 3-6 μm diameter were observed. In addition, $Lu_2Si_2O_7$ and $Lu_4Si_2N_2O_7$ were detected as the dominant crystalline phases [11]. This composition has a reported flexural strength of 687–725 MPa [5] and fracture toughness of 4.8 MPa·$m^{1/2}$ [14].

It is important to note that although NT-154 and SN-281 had a lower fracture toughness than AS-800 but the former two compositions had a lower WR. The lower wear rate of NT-154 can be attributed to the uniform grain size and lower grain boundary phase which can potentially reduce the formation of third body debris during wear testing as compared to AS-800 thus resulting in lower WR. SN-281 also showed lower WR than AS-800 which further shows that phase boundary phases are also critical factors in dry sliding behavior.

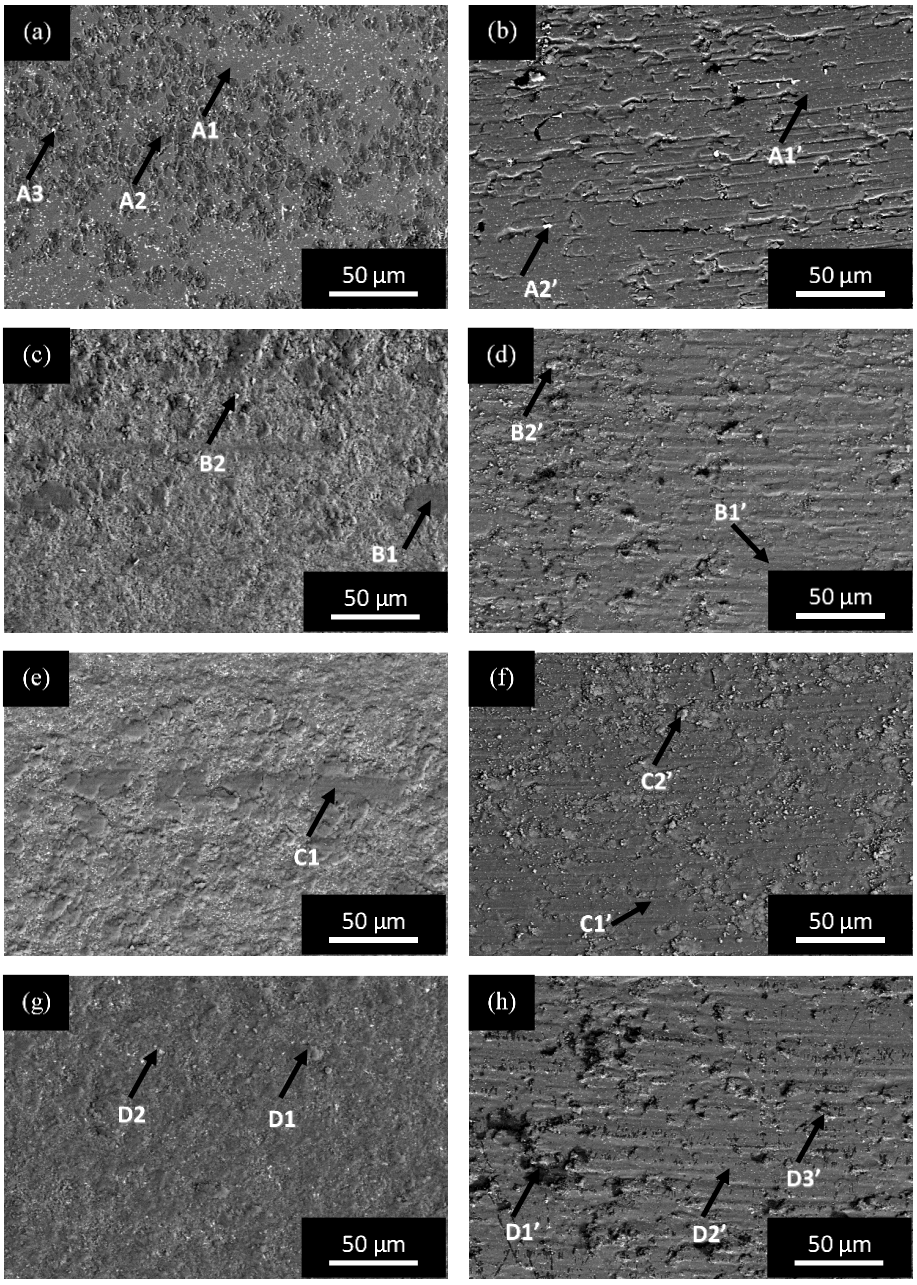

Figure 3.5 EDS of a) Hexoloy wear track, b) corresponding alumina ball counterface, c) NT-154 wear track, d) corresponding alumina ball counterface, e) SN-281 wear track, f) corresponding alumina ball counterface, g) AS-800 wear track, h) corresponding alumina ball counterface under dry sliding.

Material	Notes	Points	C	N	O	Al	Si	Lu	Y	La	Zr	O/Si ratio
Hexoloy	5 N load, Dry sliding	A1	56.34±1.46	x	0.41±0.36	x	43.34±0.51	x	x	x	x	0.009
		A2	29.59±1.04		35.04±0.94	3.29±0.17	32.09±0.43					1.092
		A3	25.90±1.39	4.22±2.11	39.99±1.31	2.22±0.22	27.66±0.47					1.446
Alumina ball	5 N load, Dry sliding	A1'	13.12±1.54	x	45.36±1.84	41.51±0.79	x	x	x	x	x	x
		A2'	14.74±1.67		21.32±1.70	27.26±0.77	8.35±0.73					0.392
NT154	5 N load, Dry sliding	B1	7.20±1.11	5.00±2.55	51.23±1.29	5.31±0.23	31.26±0.27	x	x	x	x	1.639
		B2	10.88±0.97	4.79±1.42	63.97±1.43	5.63±0.27	14.73±0.33					3.907
Alumina ball	5 N load, Dry sliding	B1'	7.08±0.78	x	53.75±1.05	39.18±0.5	x	x	x	x	x	x
		B2'	10.59±0.95	5.05±1.33	56.72±1.26	16.38±0.32	11.28±0.31					5.028
SN281	5 N load, Dry sliding	C1	8.01±0.94	5.33±1.24	58.42±1.27	7.71±0.26	20.53±0.37	x	x	x	x	2.846
		C2	8.82±0.94	5.15±1.23	44.72±1.39	3.18±0.64	28.39±0.61	4.81±0.76				1.575
Alumina ball	5 N load, Dry sliding	C1'	6.93±0.85	x	51.02±1.06	42.04±0.54	x	x	x	x	x	x
		C2'	9.42±0.99	5.59±1.63	57.44±1.26	10.74±0.26	16.73±0.33					3.433
AS800	5 N load, Dry sliding	D1	6.91±0.91	4.97±1.86	59.98±1.28	8.64±0.26	19.27±0.35	x	x	0.24±0.09	x	3.113
		D2	7.44±1.32	22.57±2.82	25.38±1.17	0.33±0.14	38.86±0.73		1.84±0.47	3.56±0.28		0.652
Alumina ball	5 N load, Dry sliding	D1'	9.39±0.81	x	51.02±1.06	39.53±0.52	x	x	x	x	x	x
		D2'	13.43±0.99		43.42±1.08	43.14±0.57						
		D3'	27.05±1.76	6.15±2.93	27.11±1.66	28.43±0.57	11.27±0.57					1.873

Table 3.1 EDS Results of Ceramics due to dry sliding

3.3.2.2 Tribology during DI water and Ethanol Lubrication

Figure 3.6 shows the wear surface after sliding in DI water. Hexoloy-alumina tribocouples showed signs of mild wear and triboxidation (E1-E3 (Table 3.2), Figs. 3.6 a-b). Li et al. [13] have also studied the tribological behavior of pressureless sintered SiC in water and observed <0.2 friction coefficient. They also observed a tribochemical reaction during the process and observed partial films of SiO_2 and $SiO_2{\cdot}nH_2O$ as SiO_2 can easily absorb H_2O [13]. The formation of smooth tribofilms can account for the high wear resistance of Hexoloy-alumina tribocouples during dry in DI water (Fig. 3.2b).

Comparatively, Si_3N_4-alumina tribocouples also showed mild wear and triboxidation which indicates DI water can be lubricating fluid in these systems (Figs. 3.6 c-h). Dante et al. [4] have proposed that formation of hydrated SiO_2 is responsible for lubricious behavior in Si_3N_4 based tribocouples. In this study, we have evaluated three different types of Si_3N_4. Based on the presented

evidence, we can propose that along with the formation of tribofilms, the chemistry of Si_3N_4 also plays an important role in the tribological behavior. In this study, AS-800 which has higher fracture toughness and different grain boundary chemistry than NT-154 showed the lowest WR. SN-281 which has 9–10 wt.% Lu_2O_3 as a sintering additive also showed higher WR than AS-800. Detailed follow up studies are recommended to understand the tribochemical behavior of different grades of Si_3N_4. Comparatively, Hexoloy performed better than different grades of Si_3N_4. Zhang et al. [3] have also summarized that self-mated SiC perform better than self-mated Si_3N_4. SiC based tribocouples have applications in mechanical seals and different tribological components like slide or thrust bearings [3]. In addition, oxide ceramics have problems like water accelerated crack growth in water which limit their applications [3]. This study shows hybrid tribocouples composed of SiC and alumina perform well during water lubrication conditions which further adds more options for design engineers.

Figure 3.7 summarizes the wear surfaces after sliding in ethanol. Hexoloy surface showed small amount of O (I1 and I2, Table 3.3) which indicates that ethanol is effective in reducing the triboxidation as compared to experiments during dry sliding and DI water lubrication. Hibi et al. [15] have also observed negligible triboxidation in ethanol lubrication in Ti_3SiC_2/SiC composites. This study shows Hexoloy can be a promising material in ethanol based tribological applications.

Dante at. [4] had reported the formation of lubricious and protective silicon alkoxide polymers which provide flattened surfaces which are effective in lowering wear rate of Si_3N_4 tribocouples. We also observed composition dependent tribological behavior where SN-281 and AS-800 performed better than NT-154 which further indicates that manufacturing process, grain structures and grain boundary chemistry played a vital role in ethanol based tribochemical process.

The formation of protective tribofilms can account for the low WR and fraction during ethanol lubrication.

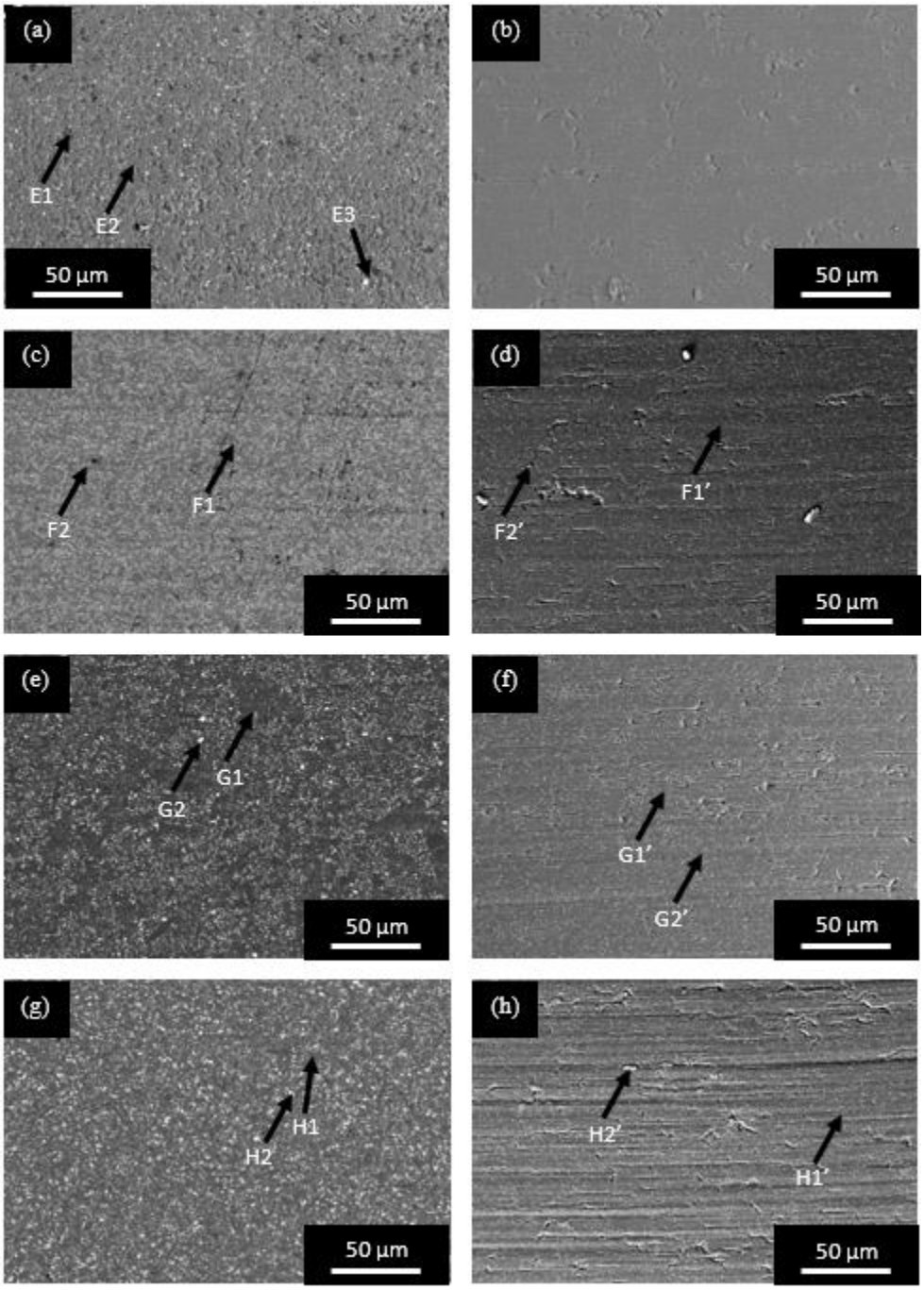

Figure 3.6 EDS of a) Hexoloy wear track, b) coresponding alumina ball counterface, c) NT-154 wear track, d) coresponding alumina ball counterface, e) SN-281 wear track, f) coresponding alumina ball counterface, g) AS-800 wear track, h) coresponding alumina ball counterface under DI water lubrication.

Material	Notes	Points	C	N	O	Al	Si	Lu	Y	La	Zr	O/Si ratio
Hexoloy	5 N load, DI water	E1	38.90±1.55	x	18.03±0.99	1.40±0.15	41.67±0.56	x	x	x	x	0.433
		E2	53.47±1.64		x	x	46.53±0.58					x
		E3	31.08±1.07		42.06±1.82	5.84±0.33	x					
NT154	5 N load, DI water	F1	14.29±1.60	35.32±2.55	3.04±1.29	x	47.35±0.59	x	x	x	x	0.064
		F2	10.97±1.55	34.23±2.60	8.28±1.38		46.53±0.60					0.178
Alumina ball	5 N load, DI water	F1'	6.80±0.80	x	52.99±1.05	40.21±0.52	x	x	x	x	x	x
		F2'	10.11±0.84		56.38±1.09	25.45±0.39	8.07±0.28					6.986
SN281	5 N load, DI water	G1	9.29±1.58	38.55±2.55	3.44±1.41	x	48.71±0.62	x	x	x	x	0.071
		G2	8.14±0.98	9.73±2.81	48.85±1.67	2.85±0.46	20.67±0.71	9.76±1.16				2.363
Alumina ball	5 N load, DI water	G1'	7.36±0.93	x	48.00±1.06	44.64±0.58	x	x	x	x	x	x
		G2'	7.51±0.97		48.13±1.08	44.36±0.58						
AS800	5 N load, DI water	H1	7.25±1.42	38.89±2.35	5.15±1.31	x	48.71±0.48	x	x	x	x	0.106
		H2	6.91±1.15	31.35±2.57	18.99±1.27	0.52±0.15	37.72±0.68		1.28±0.40	3.22±0.25		0.503
Alumina ball	5 N load, DI water	H1'	7.64±0.95	x	48.64±1.07	43.72±0.57	x	x	x	x	x	x
		H2'	10.22±0.88		54.19±1.11	24.28±0.40	11.13±0.33			0.18±0.0.06		4.869

Table 3.2 EDS Results of Ceramics due to DI water lubrication

Figure 3.8 shows schematics of dry sliding and lubricated tribological where abrasive third body was formed during former condition and lubricious film is formed during latter conditions. Comparatively, Hexoloy performed better than different grades of Si_3N_4 in both water and ethanol lubricated conditions. In addition, AS-800 showed promising behavior in both ethanol and water lubricated conditions.

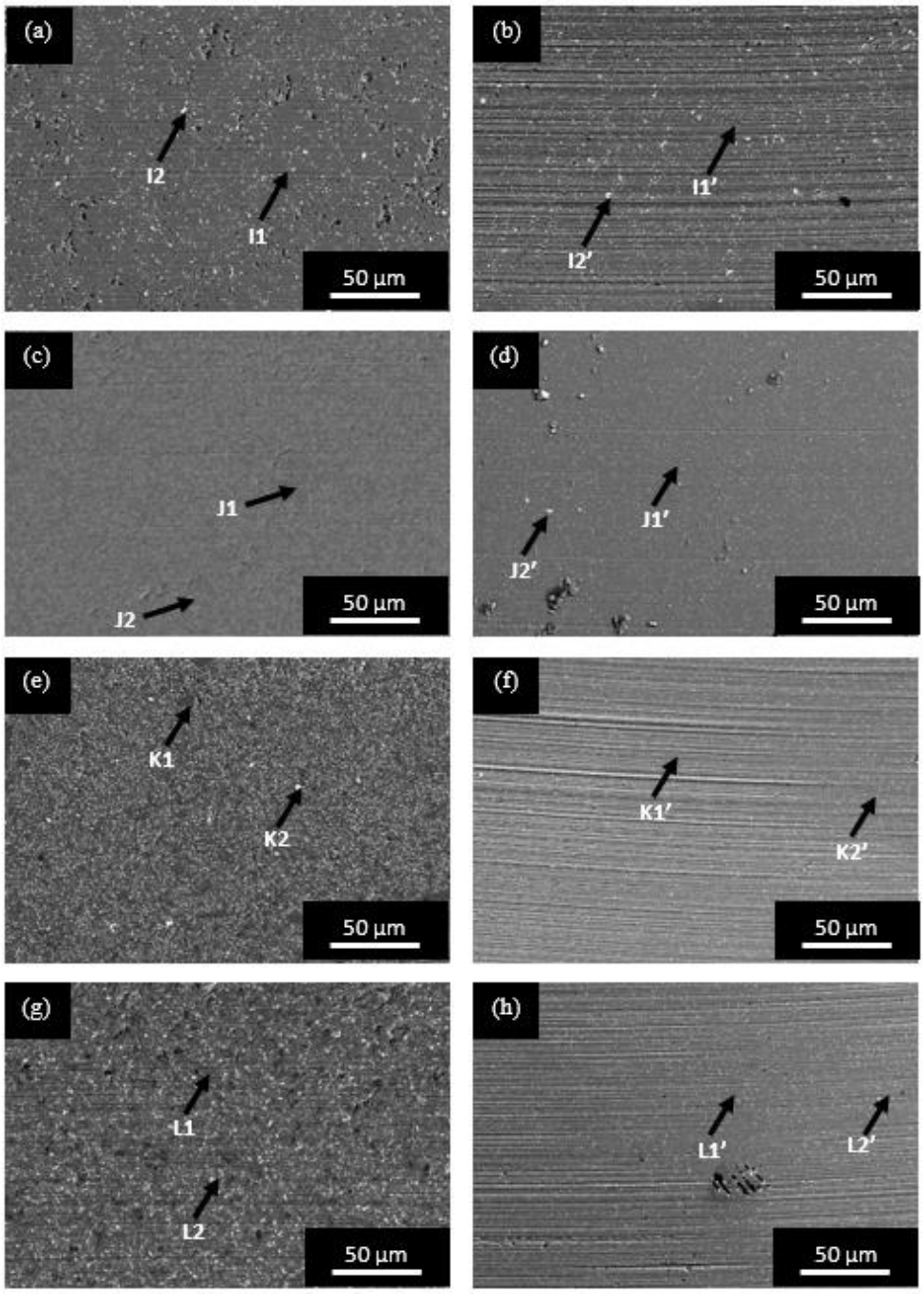

Figure 3.7 EDS of a) Hexoloy wear track, b) coresponding alumina ball counterface, c) NT-154 wear track, d) coresponding alumina ball counterface, e) SN-281 wear track, f) coresponding alumina ball counterface, g) AS-800 wear track, h) coresponding alumina ball counterface under Ethanol lubrication.

Material	Notes	Points	C	N	O	Al	Si	Lu	Y	La	Zr	O/Si ratio
Hexoloy	5 N load, Ethanol	I1	37.42±1.58	x	0.41±0.43	x	62.17±0.73	x	x	x	x	0.007
		I2	38.76±1.49		0.86±0.48		60.38±0.74					0.014
Alumina ball	5 N load, Ethanol	I1'	11.43±2.31	x	34.91±2.37	53.67±1.14	x	x	x	x	x	x
		I2'	11.84±2.37		36.53±2.47	51.63±1.15						
NT154	5 N load, Ethanol	J1	8.25±1.44	39.16±2.49	5.33±1.46	x	47.26±0.59	x	x	x	x	0.113
		J2	8.41±1.48	38.23±2.51	4.93±1.44		48.42±0.61					0.102
Alumina ball	5 N load, Ethanol	J1'	7.91±0.85	x	49.96±1.06	42.14±0.54	x	x	x	x	x	x
		J2'	7.79±1.27	3.90±2.18	52.66±1.80	24.63±0.40					11.01±0.83	
SN281	5 N load, Ethanol	K1	9.72±1.43	15.77±2.76	30.54±1.35	2.46±0.20	41.50±0.55	x	x	x	x	0.736
		K2	10.98±1.54	x	3.29±0.86	x	80.05±1.06					0.041
Alumina ball	5 N load, Ethanol	K1'	7.97±1.08	x	45.92±1.13	46.11±0.61	x	x	x	x	x	x
		K2'	16.67±2.30		45.55±1.13	46.12±0.61						
AS800	5 N load, Ethanol	L1	12.85±1.56	39.47±2.70	3.65±1.56	x	44.04±0.56	x	x	x	x	0.083
		L2	12.77±1.31	20.70±2.89	30.21±1.53		32.07±0.55			4.25±0.27		0.942
Alumina ball	5 N load, Ethanol	L1'	16.02±0.89	x	48.23±1.01	35.75±0.46	x	x	x	x	x	x
		L2'	15.08±1.06		46.23±1.14	37.14±0.50					1.55±0.46	

Table 3.3 EDS Results of Ceramics due to Ethanol lubrication

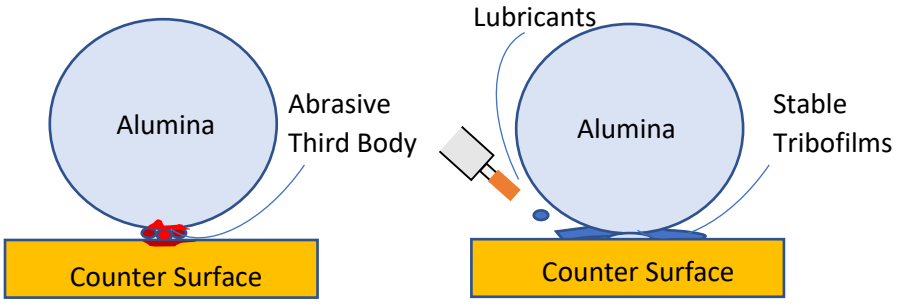

Figure 3.8 Schematics of tribological process during, (a) dry sliding and (b) in presence of lubricants (ethanol or DI water). Counter surface is either SiC or Si_3N_4

3.4 Conclusions

Tribological behavior of SiC (Hexoloy) and three different grades of Si_3N_4 namely NT-154, SN-281 and AS-800 were evaluated during dry sliding and in DI water and ethanol medium. During dry sliding, the presence of abrasive third body was responsible for the high wear rates in these compositions. Hexoloy showed a lower wear rate during ethanol and DI water lubrication due to formation of stable tribofilms which resisted the formation of third bodies. Comparatively,

Si_3N_4 samples showed lower wear rate in DI Water and ethanol. The samples also showed composition dependent behavior which indicates that grain structure and grain boundary chemistry was playing a vital role in the tribological process.

3.5 References

[1] Lim KY, Kim YW, Kim KJ. Mechanical properties of electrically conductive silicon carbide ceramics. Ceramics International. 2014;40(7):10577-10582.

[2] Zhang W. Tribology of SiC ceramics under lubrication: Features, developments, and perspectives.Current Opinion in Solid State and Materials Science. 2022;26(4):101000.

[3] Chen M, Kato K, Adachi K. The comparisons of sliding speed and normal load effect on friction coefficients of self-mated Si3N4 and SiC under water lubrication. Tribology International. 2002;35(3):129-135.

[4] Dante RC, Kajdas CK. A review and a fundamental theory of silicon nitride tribochemistry. Wear. 2012;288:27-38.

[5] Bocanegra-Bernal MH, Matovic B. Mechanical properties of silicon nitride-based ceramics and its use in structural applications at high temperatures. Materials Science and Engineering: A. 2010;527(6):1314-1338.

[6] Asthana R, Singh M. Evaluation of Pd-based brazes to join silicon nitride to copper-clad-molybdenum. Ceramics International. 2009;35(8):3511-3515.

[7] Kuszewski H, Jaworski A, Mądziel M. Lubricity of Ethanol–Diesel Fuel Blends—Study with the Four-Ball Machine Method. Materials. 2021;14(10):2492.
[8] Freedman MR. Evaluation of Silicon Nitride for Brayton Turbine Wheel Application. 2008.
[9] https://www.ceramicsrefractories.saint-gobain.com/materials/silicon-carbide-sic/hexoloy-silicon-carbide material/hexoloy-sa-sic-material
[10] Asthana R, Singh M, Martinez-Fernandez J. Joining and interface characterization of in situ reinforced silicon nitride. Journal of alloys and compounds. 2013;552:137-145.
[11] Lofaj F, Wiederhorn SM, Long GG, Hockey BJ, Jemian PR, Browder L, Andreason J, Täffner U. Non-cavitation tensile creep in Lu-doped silicon nitride. Journal of the European Ceramic Society. 2002;22(14-15):2479-2487.
[12] Zhang W, Yamashita S, Kita H. Progress in tribological research of SiC ceramics in unlubricated sliding-A review. Materials & Design. 2020;190:108528.
[13] Li JF, Huang JQ, Tan SH, Cheng ZM, Ding CX. Tribological properties of silicon carbide under water-lubricated sliding. Wear. 1998 Jul 1;218(2):167-71.
[14] Klemm H. Silicon nitride for high-temperature applications. Journal of the American Ceramic Society. 2010 Jun;93(6):1501-22.
[15] Hibi Y, Miyake K, Murakami T, Sasaki S. Tribological Behavior of SiC-Reinforced Ti3SiC2-Based Composites under Dry Condition and under Lubricated Condition with Water and Ethanol. Journal of the American Ceramic Society. 2006;89(9):2983-2985